Cellular Electrodynamics

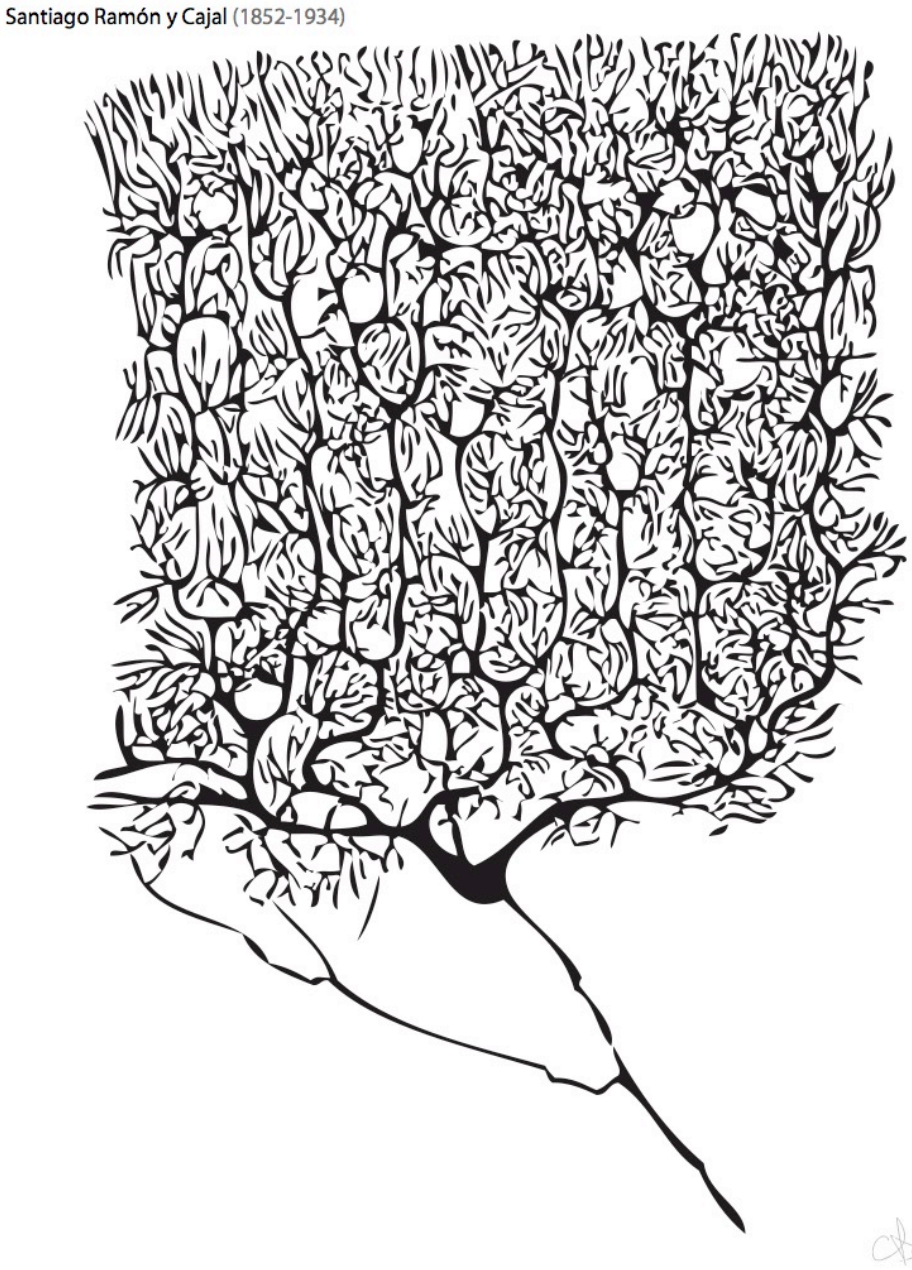

Instructor:
Prof. Christopher Bergevin (cberge@yorku.ca)

Website:
http://www.yorku.ca/cberge/4080W2020.html

York University
Winter 2020
BPHS 4080 Lecture 11

Reference/Acknowledgement:
- TF Weiss (Cellular Biophysics)
- D Freeman

Aside: Other forms of "transport" via diffusion...

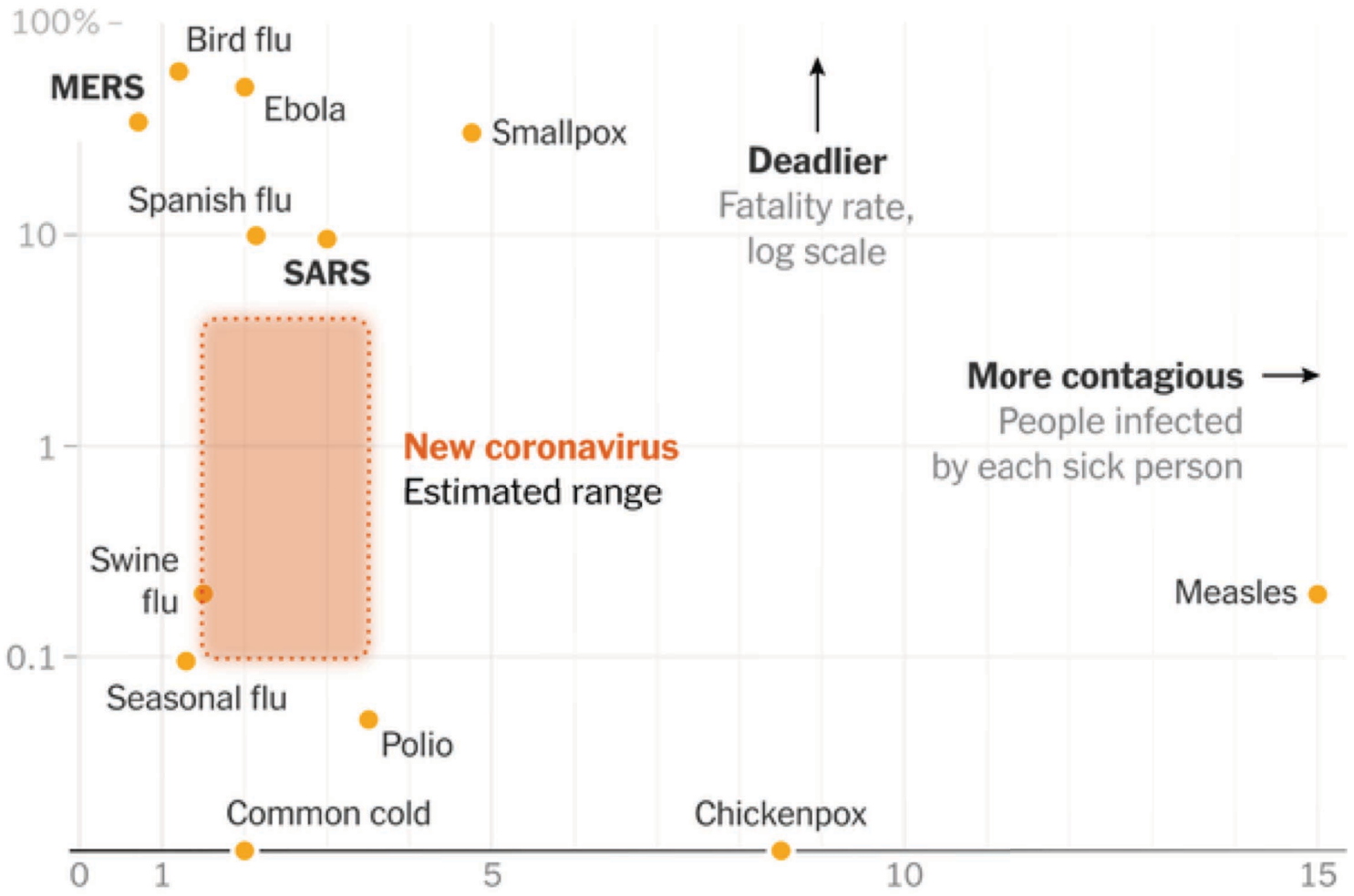

Source: New York Times (Feb. 7, 2020)

Quiz

What is different between these two “random” walkers?

Metzler & Klafter (2000)

Aside: Anomalous diffusion...

Question:
So how can we tell the difference between passive and active?

Answer:
How “normal” is your diffusion?

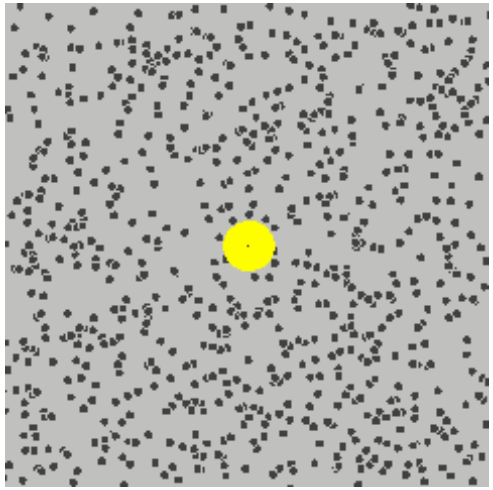

$$< x^2 > = D\,t$$

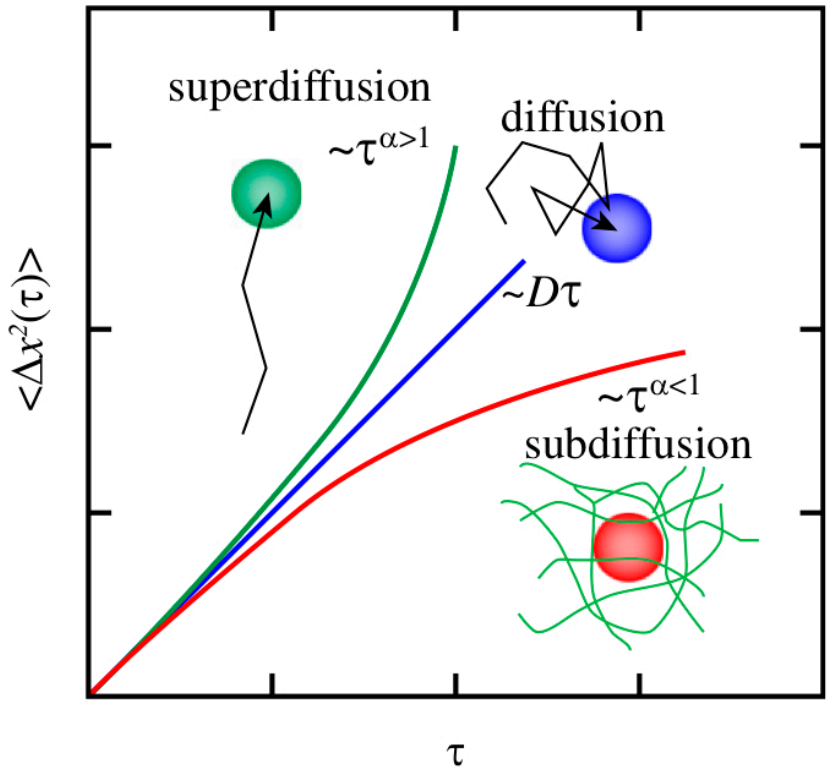

Fig. 1. Thermal diffusion (blue line) of a particle in a liquid is characterized by an MSD given by $<\Delta x^2(\tau) > = 2D\tau$, where the displacement $\Delta x(\tau) = x(t+\tau) - x(t)$ along one axis is measured over a time interval τ. In equilibrium, this linear dependence on τ is only expected for motion in simple liquids. In viscoelastic materials, such as polymer solutions, subdiffusive motion (red) is expected in equilibrium. By contrast, superdiffusive motion (green) often indicates partially or fully directed motion (e.g., for transport along a substrate) (11).

MacKintosh (PNAS 2012)

Aside: Reaction-Diffusion (or *How the leopard got its spots*)

- Chiefly just described diffusion as "flow" thus far…

Diffusion equation

$$\frac{\partial c}{\partial t} = D\frac{\partial^2 c}{\partial x^2}$$

- But addition of a "reaction" term forms a key approach to pattern formation
  (this stems from Alan Turing's famous 1952 paper *The Chemical Basis of Morphogenesis*)

Reaction-Diffusion equation

$$\frac{\partial \mathbf{c}}{\partial t} = \mathbf{f}(\mathbf{c}) + D\nabla^2\mathbf{c},$$

$\mathbf{f}(\mathbf{c})$ describes "reaction kinetics"

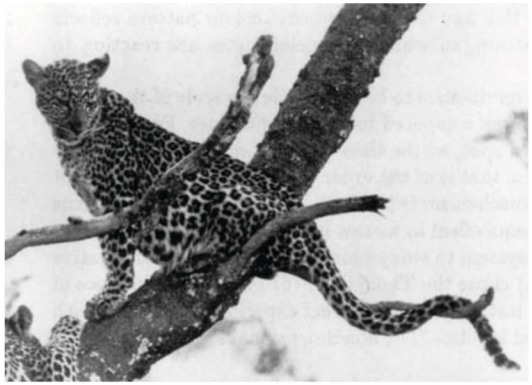

Murray (2003)

Aside: Reaction-Diffusion (or *How the leopard got its spots*)

$$\frac{\partial u}{\partial t} = \gamma f(u, v) + \nabla^2 u, \qquad \frac{\partial v}{\partial t} = \gamma g(u, v) + d\nabla^2 v$$

$$f(u, v) = a - u - h(u, v), \qquad g(u, v) = \alpha(b - v) - h(u, v)$$

$$h(u, v) = \frac{\rho u v}{1 + u + K u^2}.$$

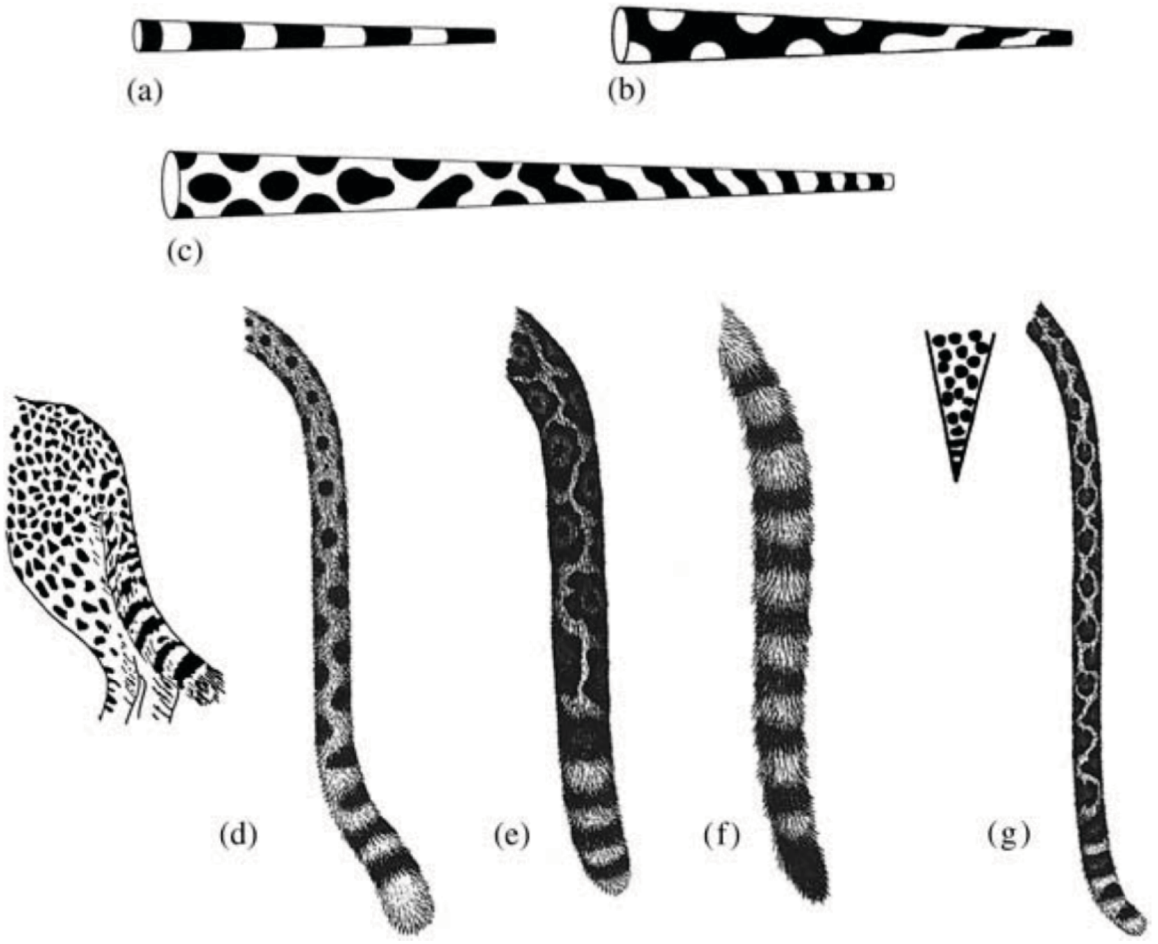

Murray (2003)

Aside: Other forms of "transport" via diffusion...

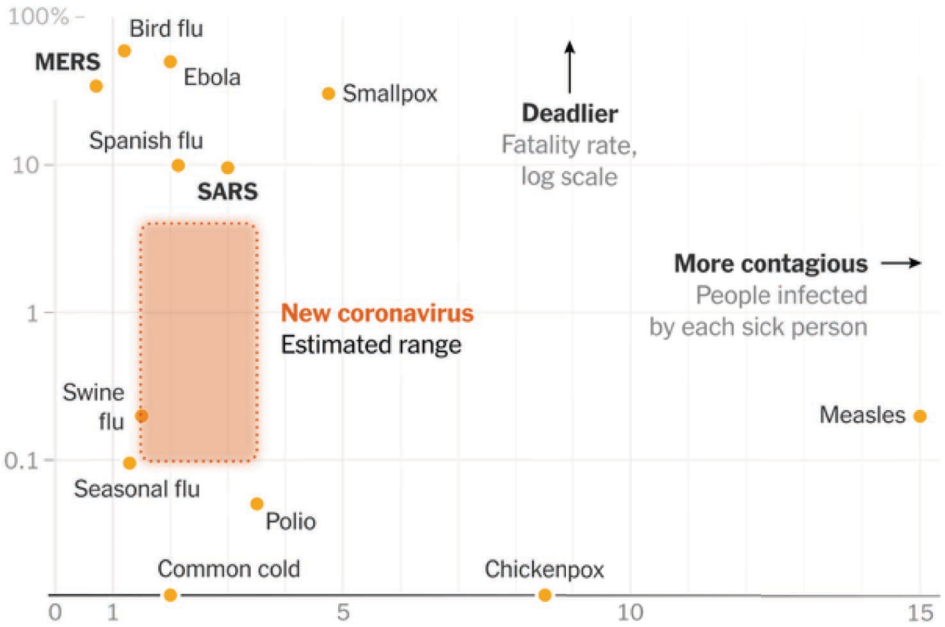

$$\frac{\partial \mathbf{c}}{\partial t} = \mathbf{f}(\mathbf{c}) + D\nabla^2\mathbf{c},$$

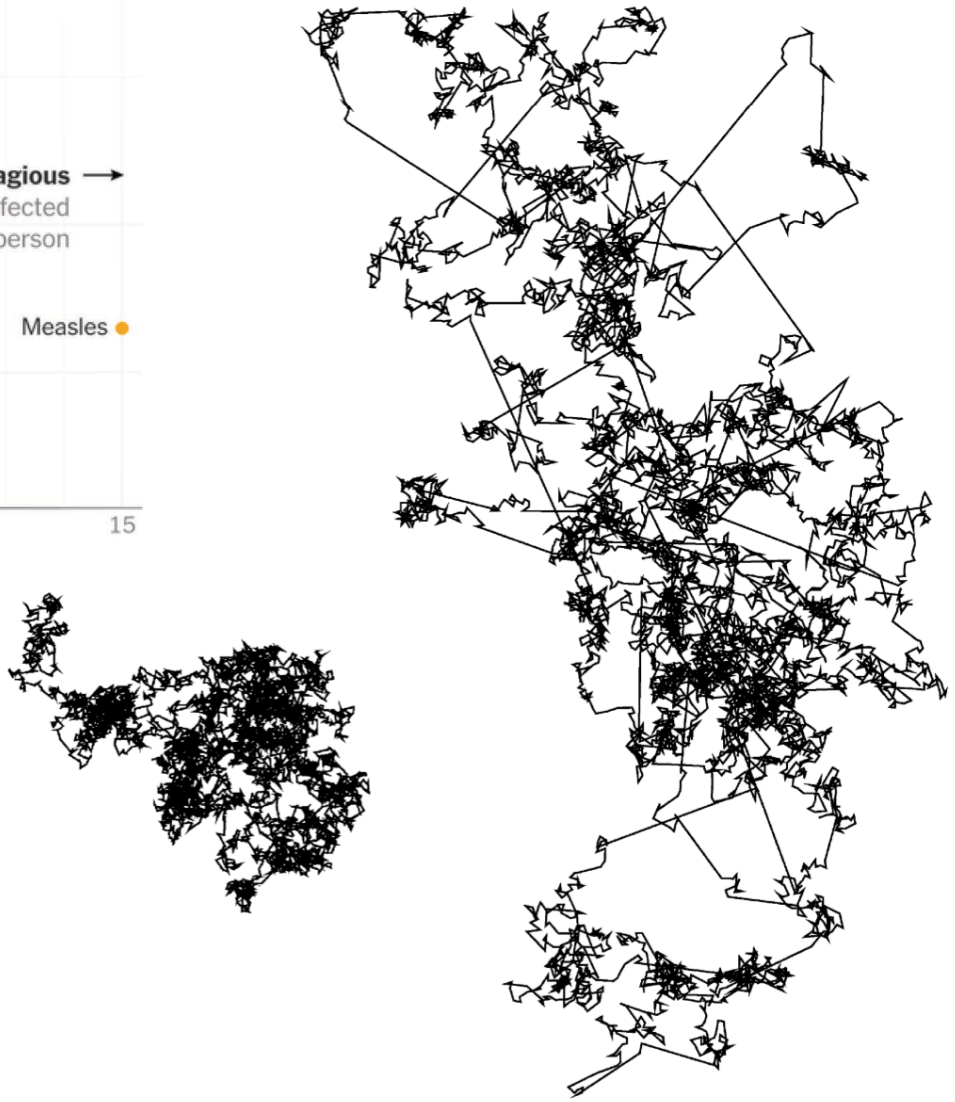

Source: New York Times (Feb. 7, 2020)

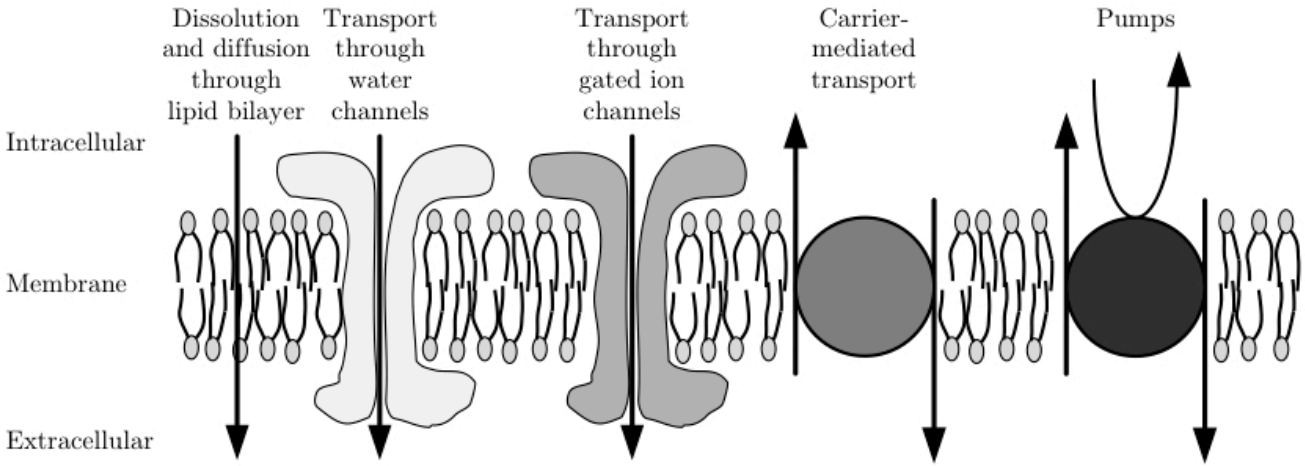

Figure 2.19

Variable conductance

(via voltage-gated ion channels)

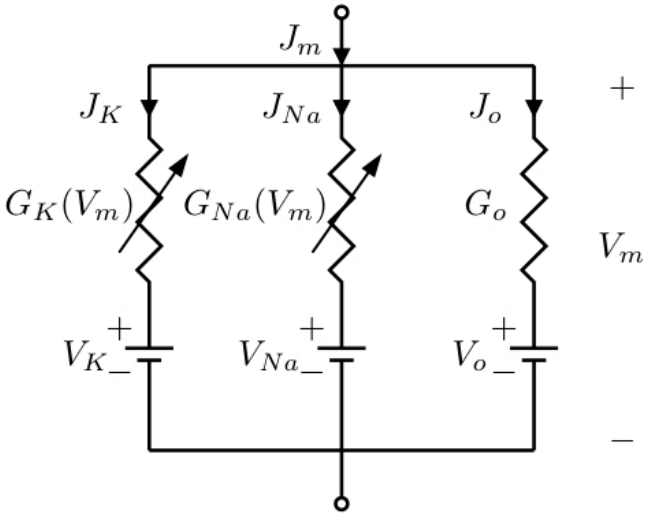

Figure 7.32

Pumps

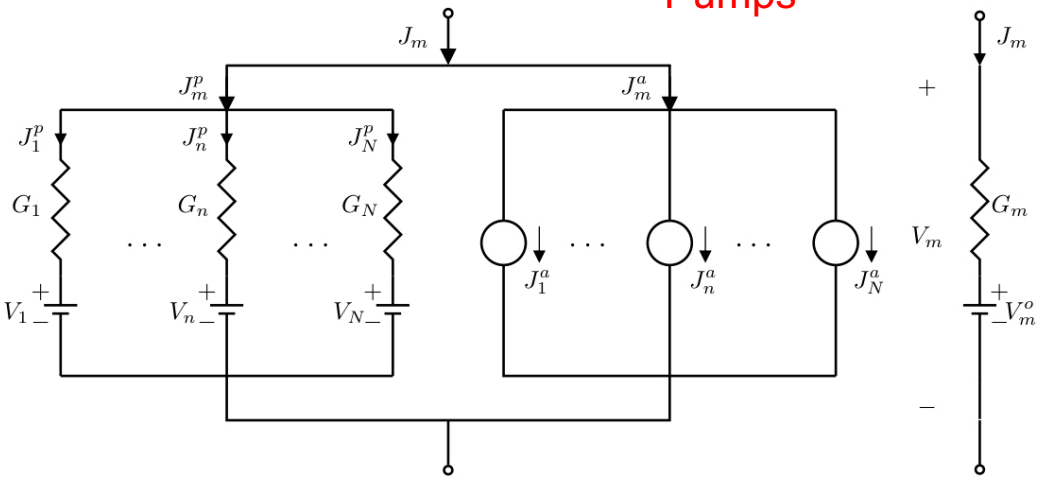

Figure 7.33

ARTICLE

doi:10.1038/nature14322

Structural basis for Na^+ transport mechanism by a light-driven Na^+ pump

Hideaki E. Kato[1]†, Keiichi Inoue[2,3,4], Rei Abe-Yoshizumi[2], Yoshitaka Kato[2], Hikaru Ono[2], Masae Konno[2], Shoko Hososhima[5,6], Toru Ishizuka[5,6], Mohammad Razuanul Hoque[5,6], Hirofumi Kunitomo[1], Jumpei Ito[7], Susumu Yoshizawa[8], Keitaro Yamashita[9], Mizuki Takemoto[1], Tomohiro Nishizawa[1], Reiya Taniguchi[1], Kazuhiro Kogure[8], Andrés D. Maturana[7], Yuichi Iino[1,6], Hiromu Yawo[5,6], Ryuichiro Ishitani[1], Hideki Kandori[2,3] & Osamu Nureki[1]

***Krokinobacter eikastus* rhodopsin 2 (KR2) is the first light-driven Na^+ pump discovered, and is viewed as a potential next-generation optogenetics tool. Since the positively charged Schiff base proton, located within the ion-conducting pathway of all light-driven ion pumps, was thought to prohibit the transport of a non-proton cation, the discovery of KR2 raised the question of how it achieves Na^+ transport. Here we present crystal structures of KR2 under neutral and acidic conditions, which represent the resting and M-like intermediate states, respectively. Structural and spectroscopic analyses revealed the gating mechanism, whereby the flipping of Asp116 sequesters the Schiff base proton from the conducting pathway to facilitate Na^+ transport. Together with the structure-based engineering of the first light-driven K^+ pumps, electrophysiological assays in mammalian neurons and behavioural assays in a nematode, our studies reveal the molecular basis for light-driven non-proton cation pumps and thus provide a framework that may advance the development of next-generation optogenetics.**

Many organisms capture light energy and information using the rhodopsin family of proteins, which comprise the heptahelical transmembrane (7-TM) proteins called opsins covalently linked to retinal. Based on their primary sequences, the opsin genes are classified into two groups: the microbial and animal opsins. The animal rhodopsins primarily work as G-protein-coupled receptors, whereas the microbial rhodopsins have divergent functions, such as ion pumps, ion channels, sensors and kinases[1–3]. Recently, the pump- and channel-type rhodopsins have attracted broad attention, since these microbial rhodopsins can be used as powerful tools in the neuroscience field to control neuronal activity in a wide range of living animals (optogenetics)[4–6].

As compared to the light-gated ion channel channelrhodopsin (ChR), the light-driven ion pumps have a long research history. Since the discoveries of the light-driven proton pump bacteriorhodopsin (BR) and the light-driven chloride pump halorhodopsin (HR)[7,8], several light-driven ion pumps, such as proteorhodopsins (PRs), xanthorhodopsin (XR), and archaerhodopsins (ARs), have been cloned and studied in diverse research fields, including optogenetics[9–12]. However, these light-driven ion pumps were basically classified into only two groups: outward proton pumps and inward chloride pumps, and no non-proton cation pumps have been discovered. Almost all of the known microbial rhodopsins are covalently bound to all-*trans* retinal (ATR) via the protonated Schiff base in the resting state, and the positively charged Schiff base proton in the middle of the ion transport pathway prevents cation transport (Extended Data Fig. 1). In the case of proton pumps, the Schiff base proton itself works as the substrate, and retinal photoisomerization alters the pK_a values of the Schiff base and the carboxylates located on the extracellular side (historically called the 'Schiff base counterions'), consequently leading to the proton transfer from the Schiff base to the extracellular side (Extended Data Fig. 1a)[3,13]. In the case of chloride pumps, Cl^- binding stabilizes the protonated Schiff base and retinal photoisomerization flips the N–H dipole, thus driving the movement of Cl^- from the extracellular environment to the intracellular side (Extended Data Fig. 1b)[3,14]. Therefore, it was widely believed that the absence of light-driven non-proton cation pumps was reasonable, because a non-proton cation would experience electrostatic repulsion from the Schiff base proton (Extended Data Fig. 1c).

However, in 2013, a new microbial rhodopsin, containing the unique NDQ (Asn112, Asp116 and Gln123) motif, was cloned from the marine flavobacterium *Krokinobacter eikastus*, and was characterized as the first light-driven Na^+ pump[15]. Although the new rhodopsin, *Krokinobacter eikastus* rhodopsin 2 (KR2), transports protons in the absence of Na^+ and Li^+, under physiological conditions it works solely as an outward Na^+ pump. A previous study revealed its cyclic photochemical reaction (photocycle) involving four spectroscopically distinguishable intermediates (K, L, M and O) and identified some of the functionally important residues[15,16], but the mechanism of Na^+ transport remained elusive. Understanding the structural basis of non-proton cation transport by KR2 would be enormously valuable, not only to enhance our knowledge of rhodopsin family proteins, but also to facilitate the design of novel light-driven ion pumps with desired ion selectivity, such as K^+ and Ca^{2+} pumps. Such ion pumps, as well as Na^+ pumps, would be useful as next-generation optogenetics tools.

Overall structure and comparison with BR

To understand the structural basis for Na^+ transport, we expressed, purified and crystallized KR2 lacking the five carboxy-terminal amino acid residues (residues 1–275). The crystals were obtained by the lipidic

[1]Department of Biological Sciences, Graduate School of Science, The University of Tokyo, 2-11-16 Yayoi, Bunkyo-ku, Tokyo 113-0032, Japan. [2]Department of Frontier Materials, Nagoya Institute of Technology, Showa-ku, Nagoya 466-8555, Japan. [3]OptoBioTechnology Research Center, Nagoya Institute of Technology, Showa-ku, Nagoya 466-8555, Japan. [4]PRESTO, Japan Science and Technology Agency, 4-1-8 Honcho, Kawaguchi, Saitama 332-0012, Japan. [5]Department of Developmental Biology and Neuroscience, Tohoku University Graduate School of Life Sciences, Sendai 980-8577, Japan. [6]CREST, Japan Science and Technology Agency, 4-1-8 Honcho, Kawaguchi, Saitama 332-0012, Japan. [7]Department of Bioengineering Sciences, Graduate School of Bioagricultural Sciences, Nagoya University, Furo-cho, Chikusa-ku, Nagoya 464-8601, Japan. [8]Atmosphere and Ocean Research Institute, The University of Tokyo, 5-1-5 Kashiwanoha, Kashiwa, Chiba 277-8564, Japan. [9]RIKEN SPring-8 Center, Hyogo 679-5148, Japan. †Present address: Department of Molecular and Cellular Physiology, Stanford University School of Medicine, Stanford, California 94305, USA.

***Krokinobacter eikastus* rhodopsin 2 (KR2) is the first light-driven Na^+ pump discovered, and is viewed as a potential next-generation optogenetics tool. Since the positively charged Schiff base proton, located within the ion-conducting pathway of all light-driven ion pumps, was thought to prohibit the transport of a non-proton cation, the discovery of KR2 raised the question of how it achieves Na^+ transport. Here we present crystal structures of KR2 under neutral and acidic conditions, which represent the resting and M-like intermediate states, respectively. Structural and spectroscopic analyses revealed the gating mechanism, whereby the flipping of Asp116 sequesters the Schiff base proton from the conducting pathway to facilitate Na^+ transport. Together with the structure-based engineering of the first light-driven K^+ pumps, electrophysiological assays in mammalian neurons and behavioural assays in a nematode, our studies reveal the molecular basis for light-driven non-proton cation pumps and thus provide a framework that may advance the development of next-generation optogenetics.**

ARTICLE

doi:10.1038/nature14322

Structural basis for Na^+ transport mechanism by a light-driven Na^+ pump

Hideaki E. Kato[1]†, Keitchi Inoue[2,3,4], Rei Abe-Yoshizumi[2], Yoshitaka Kato[2], Hikaru Ono[2], Masae Konno[2], Shoko Hososhima[5,6], Toru Ishizuka[5,6], Mohammad Razuanul Hoque[5,6], Hirofumi Kunitomo[1], Jumpei Ito[2], Susumu Yoshizawa[8], Keitaro Yamashita[9], Mizuki Takemoto[1], Tomohiro Nishizawa[1], Relya Tanigushi[1], Kazuhiro Kogure[8], Andrés D. Maturana[1], Yuichi Iino[1,6], Hiromu Yawo[5,6], Ryuichiro Ishitani[1], Hideki Kandori[2,3] & Osamu Nureki[1]

***Krokinobacter eikastus* rhodopsin 2 (KR2) is the first light-driven Na^+ pump discovered, and is viewed as a potential next-generation optogenetics tool. Since the positively charged Schiff base proton, located within the ion-conducting pathway of all light-driven ion pumps, was thought to prohibit the transport of a non-proton cation, the discovery of KR2 raised the question of how it achieves Na^+ transport. Here we present crystal structures of KR2 under neutral and acidic conditions, which represent the resting and M-like intermediate states, respectively. Structural and spectroscopic analyses revealed the gating mechanism, whereby the flipping of Asp116 sequesters the Schiff base proton from the conducting pathway to facilitate Na^+ transport. Together with the structure-based engineering of the first light-driven K^+ pumps, electrophysiological assays in mammalian neurons and behavioural assays in a nematode, our studies reveal the molecular basis for light-driven non-proton cation pumps and thus provide a framework that may advance the development of next-generation optogenetics.**

Many organisms capture light energy and information using the rhodopsin family of proteins, which comprise the heptahelical transmembrane (7-TM) proteins called opsins covalently linked to retinal. Based on their primary sequences, the opsin genes are classified into two groups: the microbial and animal opsins. The animal rhodopsins primarily work as G-protein-coupled receptors, whereas the microbial rhodopsins have divergent functions, such as ion pumps, ion channels, sensors and kinases[1–3]. Recently, the pump- and channel-type rhodopsins have attracted broad attention, since these microbial rhodopsins can be used as powerful tools in the neuroscience field to control neuronal activity in a wide range of living animals (optogenetics)[4–6].

As compared to the light-gated ion channel channelrhodopsin (ChR), the light-driven ion pumps have a long research history. Since the discoveries of the light-driven proton pump bacteriorhodopsin (BR) and the light-driven chloride pump halorhodopsin (HR)[7,8], several light-driven ion pumps, such as proteorhodopsins (PRs), xanthorhodopsin (XR), and archaerhodopsins (ARs), have been cloned and studied in diverse research fields, including optogenetics[9–13]. However, these light-driven ion pumps were basically classified into only two groups: outward proton pumps and inward chloride pumps, and no non-proton cation pumps have been discovered. Almost all of the known microbial rhodopsins are covalently bound to all-*trans* retinal (ATR) via the protonated Schiff base in the resting state, and the positively charged Schiff base proton in the middle of the ion transport pathway prevents cation transport (Extended Data Fig. 1). In the case of proton pumps, the Schiff base proton itself works as the substrate, and retinal photoisomerization alters the pK_a values of the Schiff base and the carboxylates located on the extracellular side (historically called the 'Schiff base counterions'), consequently leading to the proton transfer from the Schiff base to the extracellular side (Extended Data Fig. 1a)[3,13]. In the case of chloride pumps, Cl^- binding stabilizes the protonated Schiff base and retinal photoisomerization flips the N–H dipole, thus driving the movement of Cl^- from the extracellular environment to the intracellular side (Extended Data Fig. 1b)[7,14]. Therefore, it was widely believed that the absence of light-driven non-proton cation pumps was reasonable, because a non-proton cation would experience electrostatic repulsion from the Schiff base proton (Extended Data Fig. 1c).

However, in 2013, a new microbial rhodopsin, containing the unique NDQ (Asn112, Asp116 and Gln123) motif, was cloned from the marine flavobacterium *Krokinobacter eikastus*, and was characterized as the first light-driven Na^+ pump[15]. Although the new rhodopsin, *Krokinobacter eikastus* rhodopsin 2 (KR2), transports protons in the absence of Na^+ and Li^+, under physiological conditions it works solely as an outward Na^+ pump. A previous study revealed its cyclic photochemical reaction (photocycle) involving four spectroscopically distinguishable intermediates (K, L, M and O) and identified some of the functionally important residues[15,16], but the mechanism of Na^+ transport remained elusive. Understanding the structural basis of non-proton cation transport by KR2 would be enormously valuable, not only to enhance our knowledge of rhodopsin family proteins, but also to facilitate the design of novel light-driven ion pumps with desired ion selectivity, such as K^+ and Ca^{2+} pumps. Such ion pumps, as well as Na^+ pumps, would be useful as next-generation optogenetics tools.

Overall structure and comparison with BR

To understand the structural basis for Na^+ transport, we expressed, purified and crystallized KR2 lacking the five carboxy-terminal amino acid residues (residues 1–275). The crystals were obtained by the lipidic

[1]Department of Biological Sciences, Graduate School of Science, The University of Tokyo, 2-11-16 Yayoi, Bunkyo-ku, Tokyo 113-0032, Japan. [2]Department of Frontier Materials, Nagoya Institute of Technology, Showa-ku, Nagoya 466-8555, Japan. [3]OptoBioTechnology Research Center, Nagoya Institute of Technology, Showa-ku, Nagoya 466-8555, Japan. [4]PRESTO, Japan Science and Technology Agency, 4-1-8 Honcho, Kawaguchi, Saitama 332-0012, Japan. [5]Department of Developmental Biology and Neuroscience, Tohoku University Graduate School of Life Sciences, Sendai 980-8577, Japan. [6]CREST, Japan Science and Technology Agency, 4-1-8 Honcho, Kawaguchi, Saitama 332-0012, Japan. [7]Department of Bioengineering Sciences, Graduate School of Bioagricultural Sciences, Nagoya University, Furo-cho, Chikusa-ku, Nagoya 464-8601, Japan. [8]Atmosphere and Ocean Research Institute, The University of Tokyo, 5-1-5 Kashiwanoha, Kashiwa, Chiba 277-8564, Japan. [9]RIKEN SPring-8 Center, Hyogo 679-5148, Japan. †Present address: Department of Molecular and Cellular Physiology, Stanford University School of Medicine, Stanford, California 94305, USA.

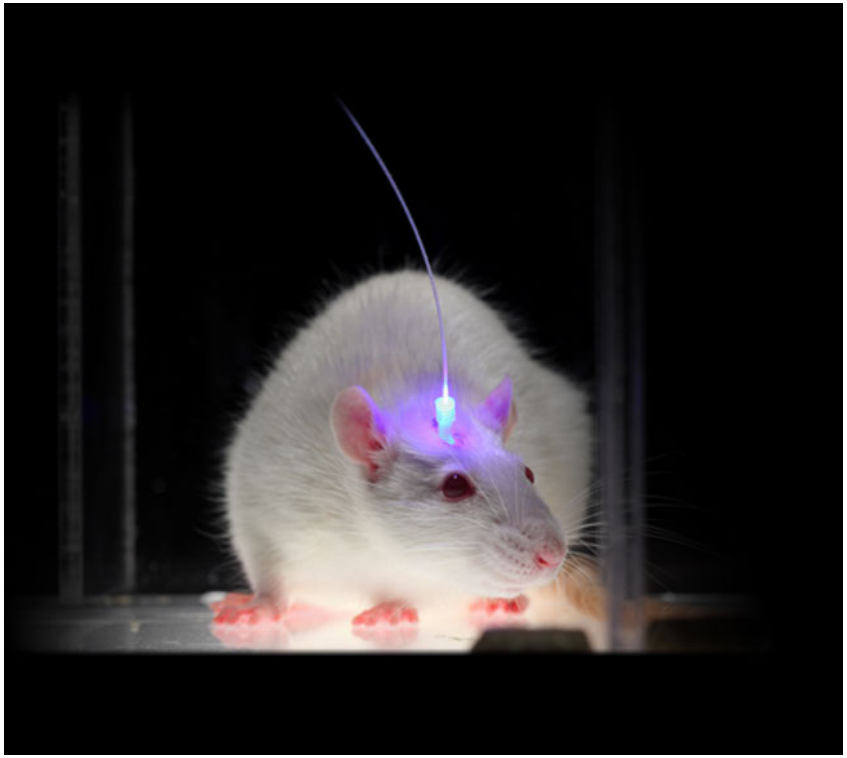

http://web.stanford.edu/group/dlab/optogenetics/

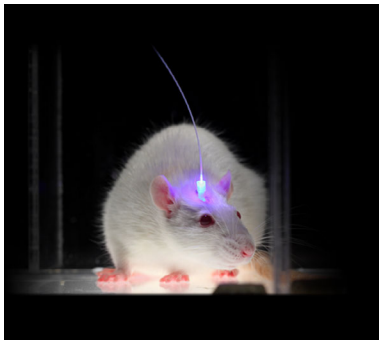

How optogenetics works

A light-sensitive protein from algae

Take the gene for this protein...

... and insert the DNA into specific neurons in the brain

This protein is an ion channel that opens in response to **blue light**

Neurons communicate by "**firing**." This is an electrical signal created by opening & closing ion channels.

So now you can cause neurons to fire just by flashing **blue light!**

With the right combination of neurons, you can activate an entire brain circuit to control specific behaviors (like movement)

http://neurobyn.blogspot.ca/2011/01/controlling-brain-with-lasers.html

Structural basis for Na^+ transport mechanism by a light-driven Na^+ pump

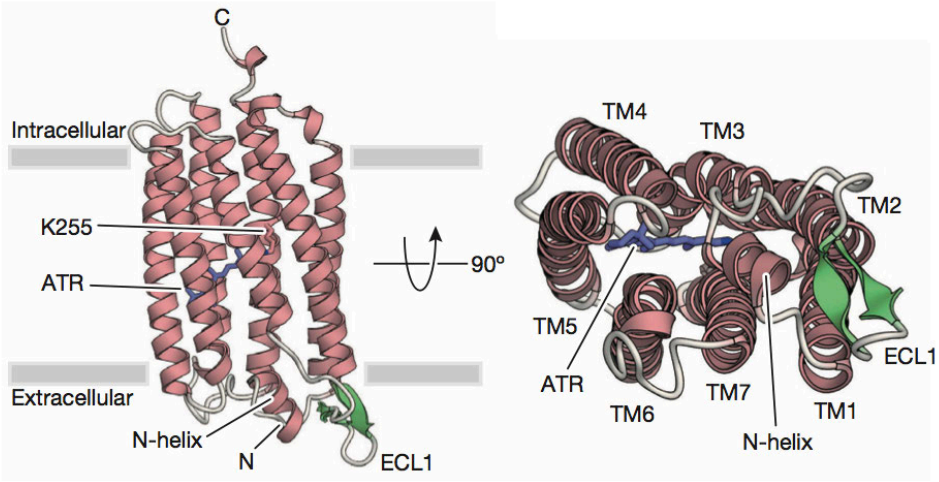

Figure 1 | Overall structure of KR2 and comparison with BR. Crystal structure of KR2, viewed parallel to the membrane (left), and from the extracellular side (right). KR2 consists of the N-helix and the seven transmembrane helices (TM1–TM7) connected by extracellular loops (ECL1–ECL3) and intracellular loops (ICL1–ICL3). ATR, depicted by stick models, is coloured blue, and ECL1 is coloured green.

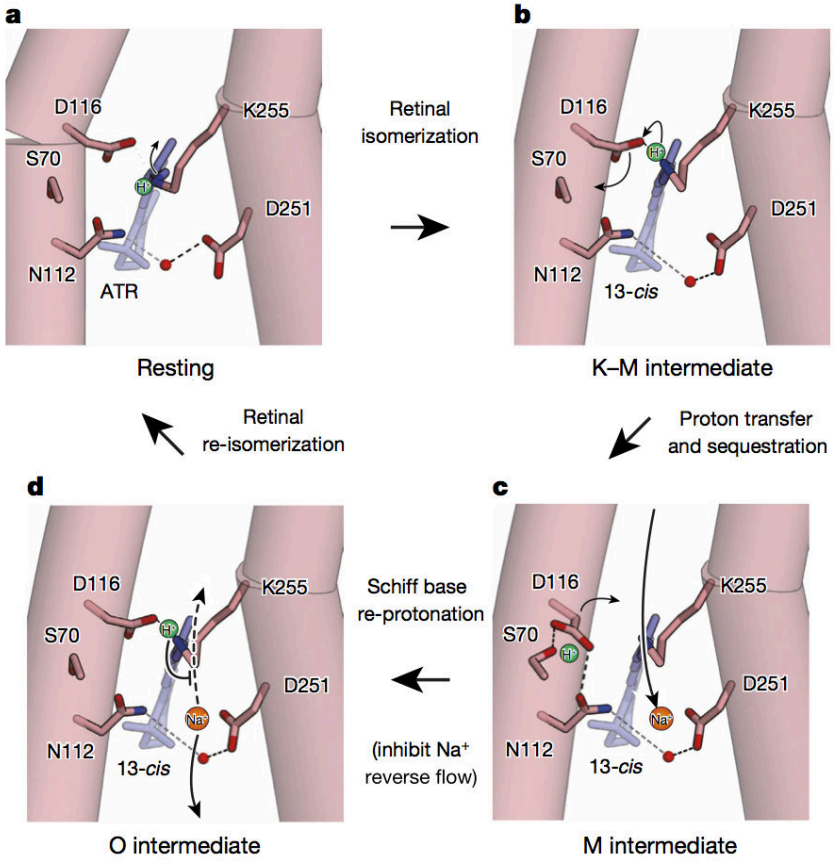

Figure 5 | Proposed model of Na^+ transport. The water, proton and Na^+ are depicted by the red, green and orange spheres, respectively. **a**, In the resting state, the positive charge of the Schiff base proton blocks Na^+ transport. **b**, After retinal isomerization and N–H flipping, the Schiff base proton is transferred to Asp116. **c**, In the M intermediate, the protonated Asp116 flips away and forms hydrogen bonds with Ser70 and Asn112. The flipping of Asp116 reduces the energy barrier to Na^+ transport, and thereby facilitates the Na^+ conduction. **d**, The re-protonation of the Schiff base would inhibit the reverse flow of Na^+.

Structural basis for Na^+ transport mechanism by a light-driven Na^+ pump

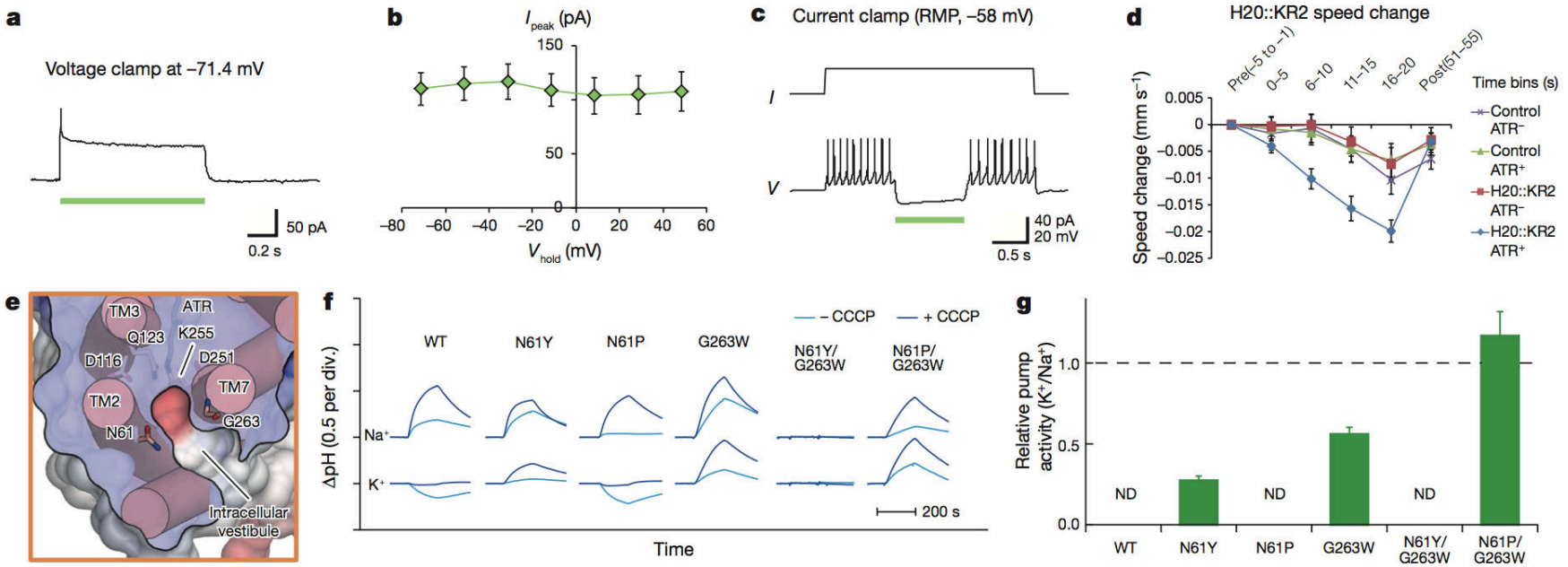

Figure 6 | Optogenetic applications and molecular engineering of KR2. **a-c**, Electrophysiology in cortical neurons. **a**, Voltage-clamp recording of the KR2 photocurrent. **b**, The current–voltage relationship. Values are means ± s.e.m. of 10 experiments. **c**, Current-clamp recording. Light illumination (green bar) inhibited the generation of the action potential. RMP, resting membrane potential. **d**, Effect of KR2 activation on *C. elegans* locomotion behaviour. The plot shows the change in the motion speed during and after light illumination (mean ± s.e.m., $n = 9–10$). **e**, Transverse section from the intracellular side. **f**, Pump activities of wild-type (WT) KR2 and mutants in *E. coli* cells suspended in 100 mM NaCl (top) or KCl (bottom), without (light blue) and with (dark blue) CCCP. Each tick mark of the *y* axis represents 0.5 pH change. **g**, Ion selectivities of wild-type KR2 and mutants. Values are means and standard deviation (s.d.) of three experiments. ND, not detected.

→ Note some terms here ("voltage clamp", "current clamp", I-V relation) we will return to....

Looking Ahead: Hodgkin-Huxley network

Figure 4.7 (vol.2)

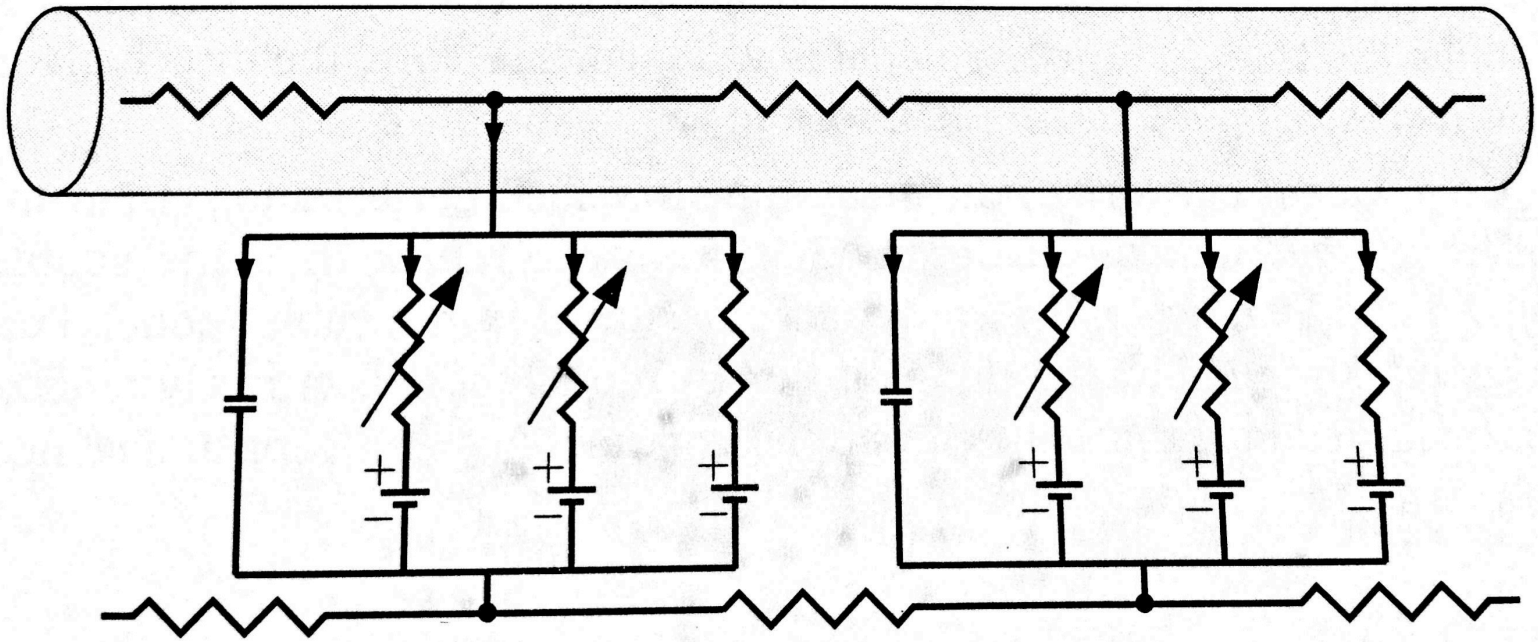

Two main ingredients:

- "sections" of membrane behaving like parallel circuit w/ variable conductances & a capacitor
- successive elements spatially arranged like a "transmission line"

Electrical Properties of Cells

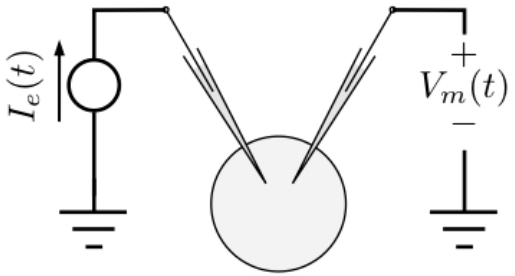

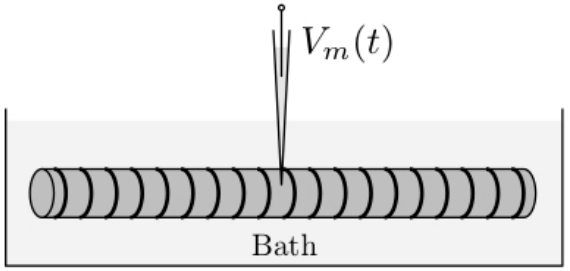

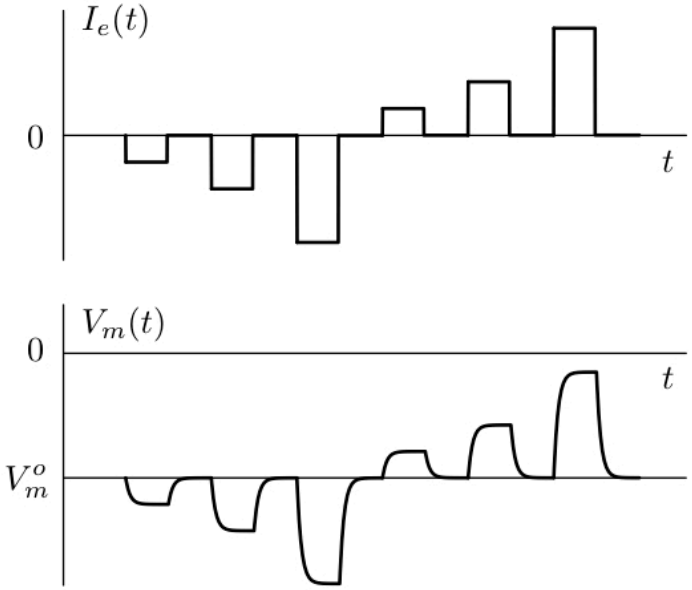

Figure 1.1

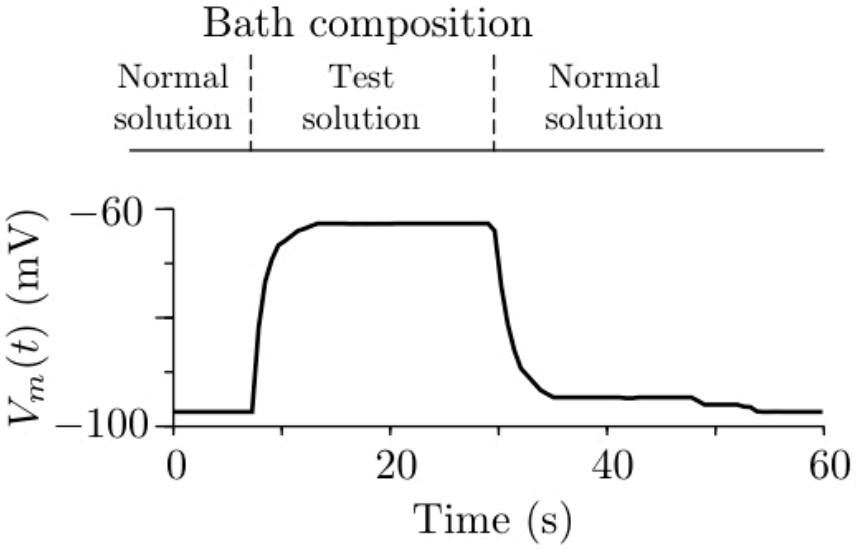

Figure 1.2

Graded potentials (note RC time constant!)

Extracellular solution can have a big effect

Electrical Properties of Cells → How to measure?

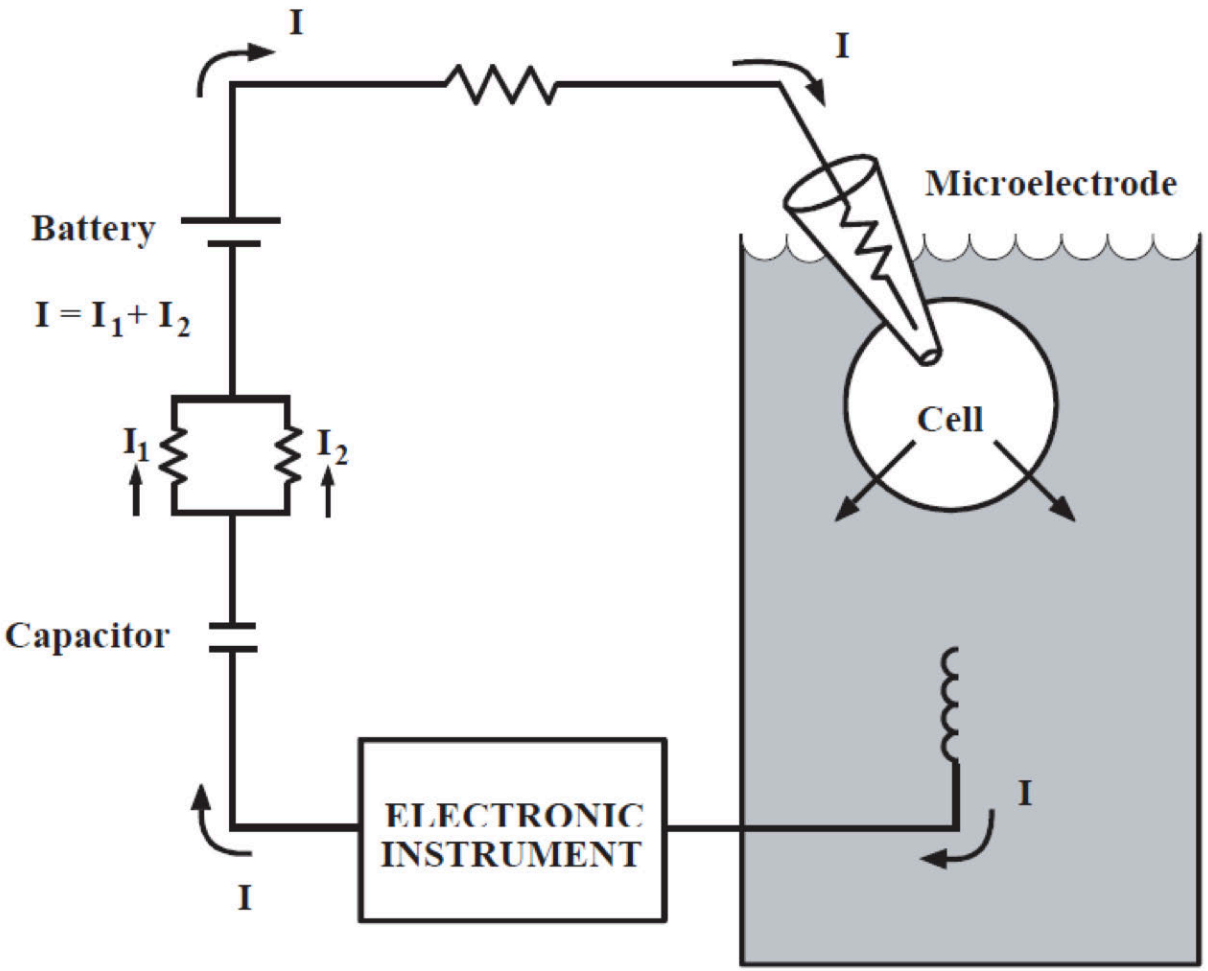

Figure 1-2 A typical electrical circuit. Example of an electrical circuit with various parts. Current always flows in a complete circuit.

http://ala-laurila.biosci.helsinki.fi/content/refs/axon_guide_3rd_edition.pdf

Electrical Properties of Cells → How to measure?

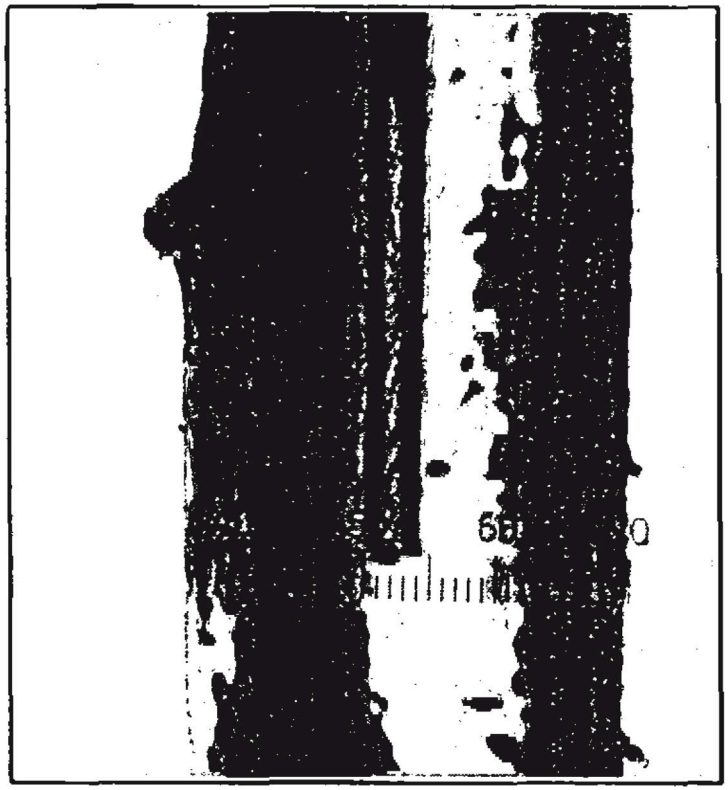

Fig. 1.

PHOTOMICROGRAPH OF ELECTRODE INSIDE GIANT AXON. 1 SCALE DIVISION = 33 μ.

in approximate calculations, so that we may write for (1) and (2):

$$V = \frac{2Kc}{c^2 - 4kd} \quad . \quad . \quad . \quad . \quad . \quad (6)$$

$$\text{and} \quad k_1 = c/2, \quad . \quad . \quad . \quad . \quad . \quad (7)$$

From equations 6 and 7 it appears that as potassium is substituted for sodium in the external solution, the potassium concentration in the cell will remain unchanged, but potassium will enter and the cell volume increase. As the external concentration is increased, the potassium concentration inside will increase; but if the external potassium is also raised, the volume will stand higher than otherwise and potassium will have entered the cell.

When excised muscle is immersed in Ringer or Barkan fluid, potassium is lost until the external potassium is 29 milliequiv./litre. The raised equilibrium value appears associated with widening of the cation and anion pores, and it is from this raised value we shall consider the effect of potassium changes. The interspace fluid is taken as 9 ml./100 gm. tissue (from magnesium and inulin methods), though small differences with total volume changes will not materially affect the calculations.

The following table illustrates the kind of results obtained; each figure being the mean of four or five experiments. Concentrations are expressed as milliequiv./litre of external fluid or 'fibre' water (which latter is normally 71 ml./100 gm. muscle).

Potassium conc. in ext. fluid	Total conc. of ext. fluid	Potassium conc. of 'fibre' water Exper.	Theor.	Potassium entry. Millicquiv./litre of 'fibre' water
2·5	240 (plasma)	119	120	
33·5	248	115	124	12·5
103	256	121	128	83·8
103	384	196	192	33·2
103	534	263	267	8·8

For equation 3 we have the following data, taking chloride as an example of the permeable anion.

External conc.		Inside conc.		Products	
K	Cl	K	Cl	K × Cl	K × Cl
29	100	119	26·6	3074	3165
80·4	132	145	73·0	10613	10585

Original entrance of potassium and relation of potassium interchanges to carbohydrate metabolism. Here we shall consider briefly an apparently easy and effective means of increasing the potassium in cells without change in external potassium or in total concentration outside. If, in the above scheme, impermeable anions are formed from permeable, V the volume of the cell will increase from equation 6, and potassium and more diffusible anion will enter the cell in accordance with equations 3, 2 or 7. No intermediation of hydrogen ion with its excessively low gradients will be necessary. A permeable anion that could play this part pre-eminently is phosphate, and when we examine the nature of the impermeable non-colloidal anions within the fibre we find that they are mostly if not quite formed of phosphorylated compounds important for the carbohydrate cycle. If such compounds decrease in concentration during rapid carbohydrate oxidation, potassium should leave the cell, and when reformed the reverse should occur. A relation between carbohydrate metabolism and potassium interchanges has, in fact, been already noted (for example, by Verzar) and is here rationally interpreted.

With the above membrane the potential changes with varying external solutions can also be readily understood, previous explanations assuming chloride impermeability being demonstrably incorrect.

The above research was supported by a grant from the Irish Medical Research Council.

E. J. CONWAY.
P. J. BOYLE.
University College,
Dublin.
Sept. 1.

Action Potentials Recorded from Inside a Nerve Fibre

NERVOUS messages are invariably associated with an electrical change known as the action potential. This potential is generally believed to arise at a membrane which is situated between the axoplasm and the external medium. If this theory is correct, it should be possible to record the action potential between an electrode inside a nerve fibre and the conducting fluid outside it. Most nerve fibres are too small for this to be tested directly, but we have recently succeeded in inserting micro-electrodes into the giant axons of squids (*Loligo forbesi*)[1].

The following method was used. A 500 μ axon was partially dissected from the first stellar nerve and cut half through with sharp scissors. A fine cannula was pushed through the cut and tied into the axon with a thread of silk. The cannula was mounted with the axon hanging from it in sea water. The upper part of the axon was illuminated from behind and could be observed from the front and side by means of a system of mirrors and a microscope; the lower part was insulated by oil and could be stimulated electrically. Action potentials were recorded by connecting one amplifier lead to the sea water outside the axon and the other to a micro-electrode which

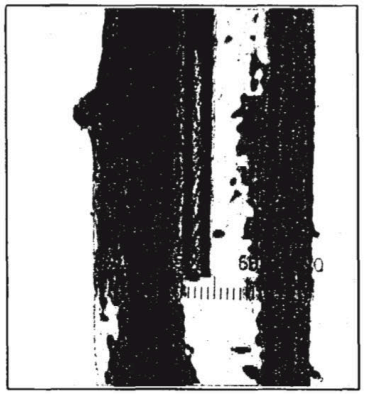

Fig. 1.

PHOTOMICROGRAPH OF ELECTRODE INSIDE GIANT AXON. 1 SCALE DIVISION = 33 μ.

Electrical Properties of Cells → How to measure?

Fig. 1.

PHOTOMICROGRAPH OF ELECTRODE INSIDE GIANT AXON. 1 SCALE DIVISION = 33 μ.

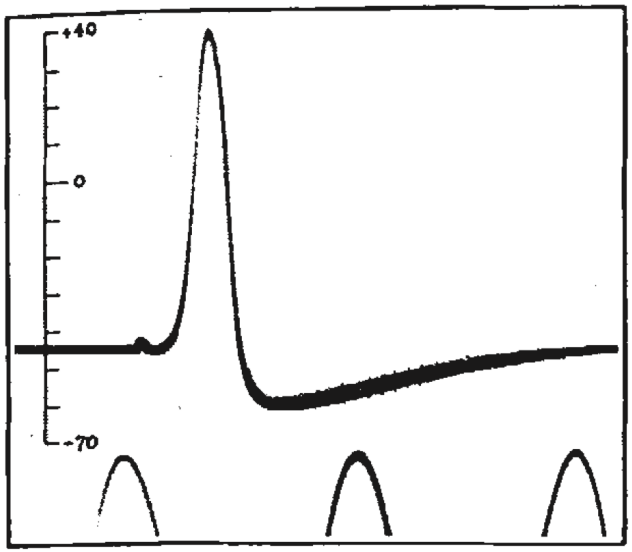

Fig. 2.

ACTION POTENTIAL RECORDED BETWEEN INSIDE AND OUTSIDE OF AXON. TIME MARKER, 500 CYCLES/SEC. THE VERTICAL SCALE INDICATES THE POTENTIAL OF THE INTERNAL ELECTRODE IN MILLIVOLTS, THE SEA WATER OUTSIDE BEING TAKEN AT ZERO POTENTIAL.

→ First direct measurement of an action potential!

Hodgkin & Huxley (1939)

Electrical Responses in Sensory Systems

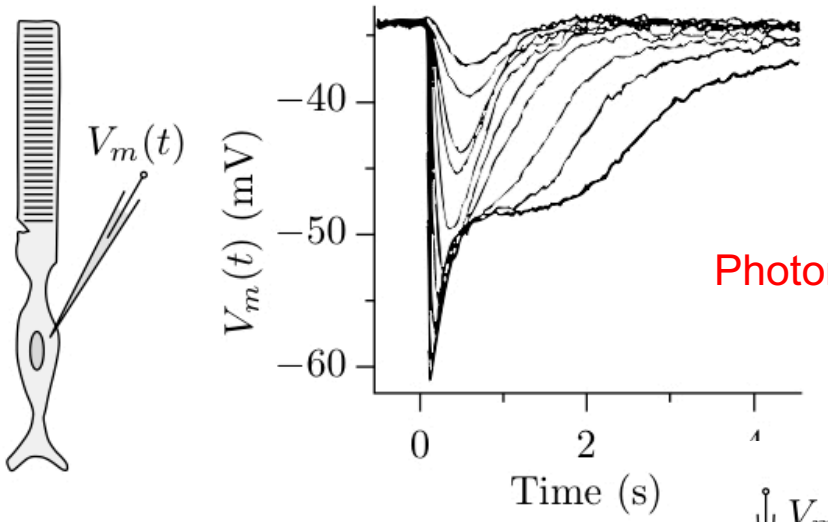

Photoreceptors

Figure 1.3

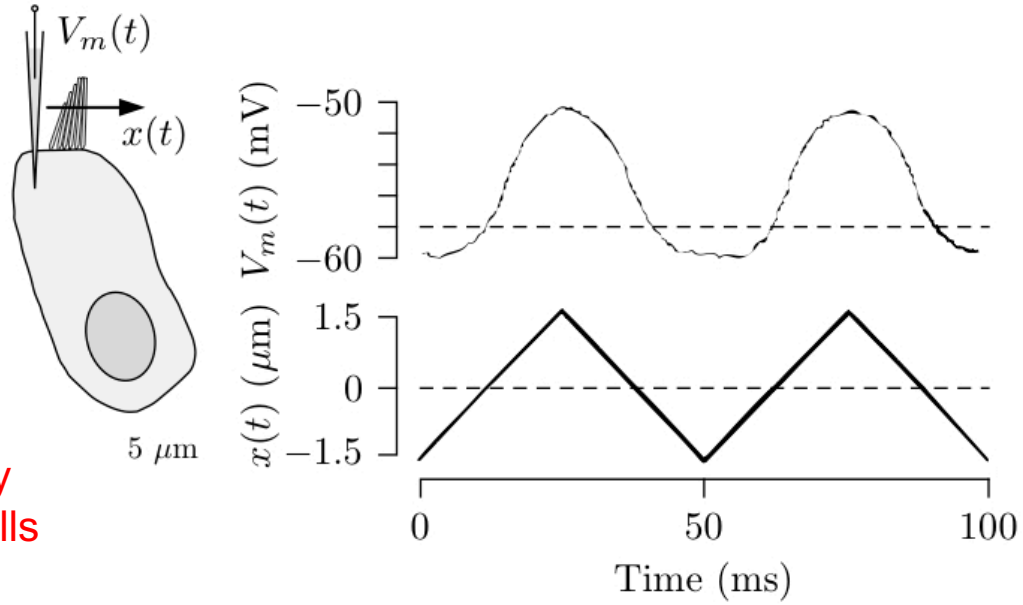

Auditory Hair Cells

Figure 1.5

Electrical Responses in Sensory Systems

Mechanoreceptors

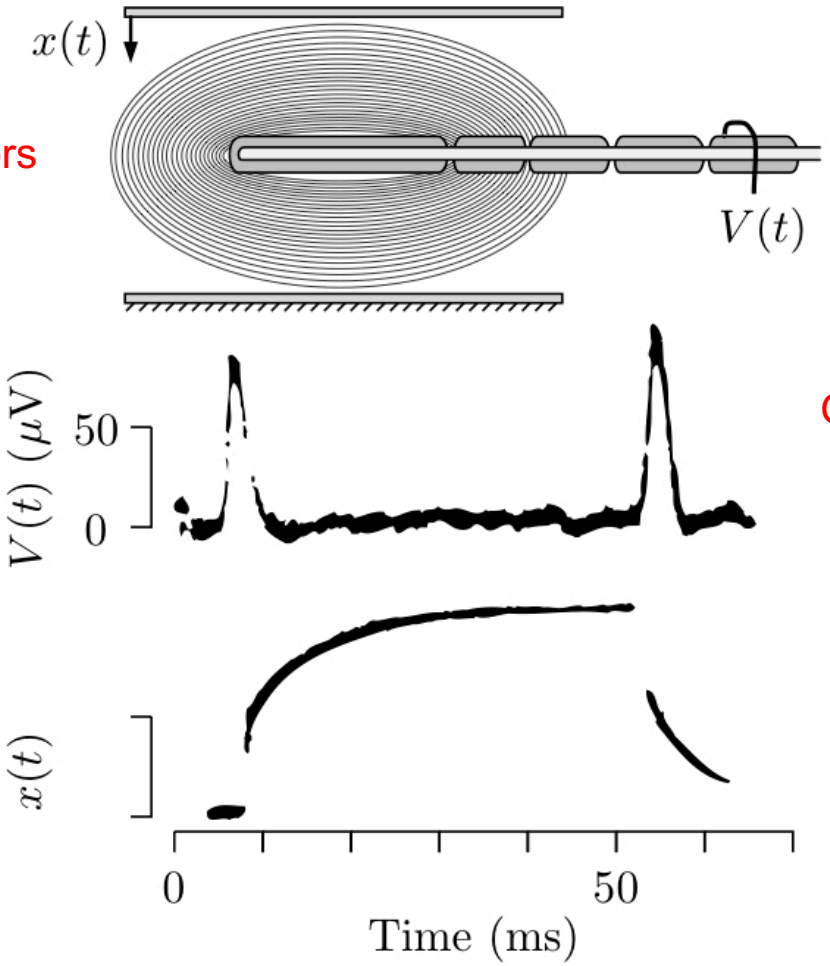

Graded potential (w/ adaptation)

(not an action potential)

Figure 1.4

Electrical Responses in Sensory Systems

Chemoreceptors (taste)

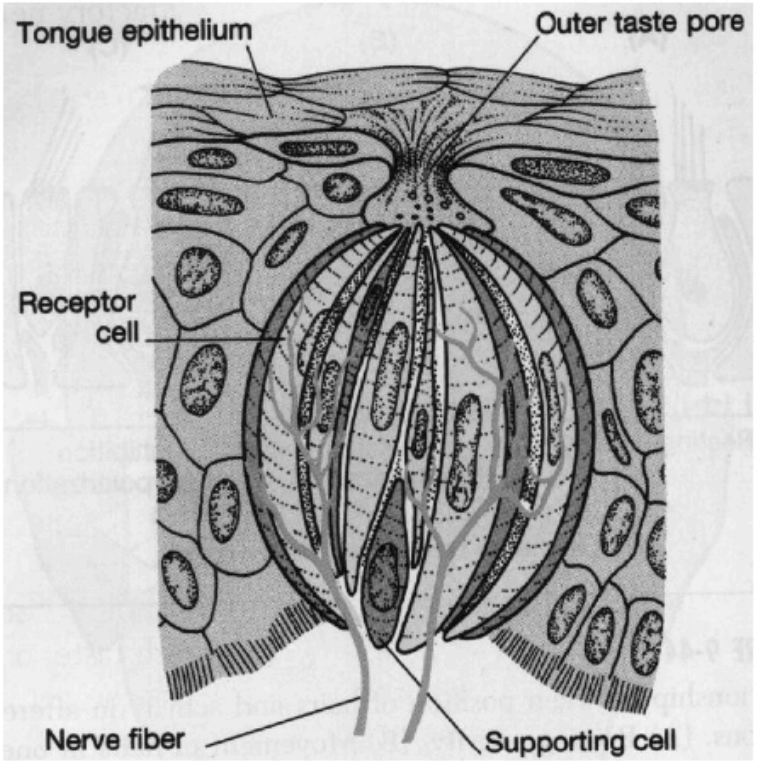

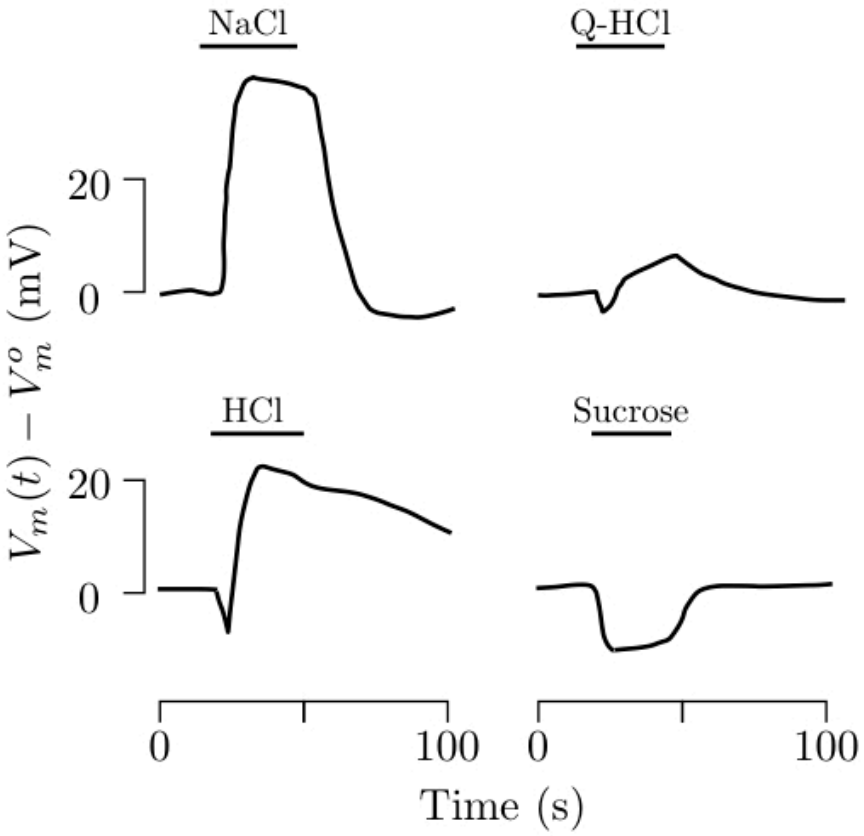

Figure 1.6

Electrical Responses in Sensory Systems

Chemoreceptors (chemical synapse) → "Neurotransmitters"

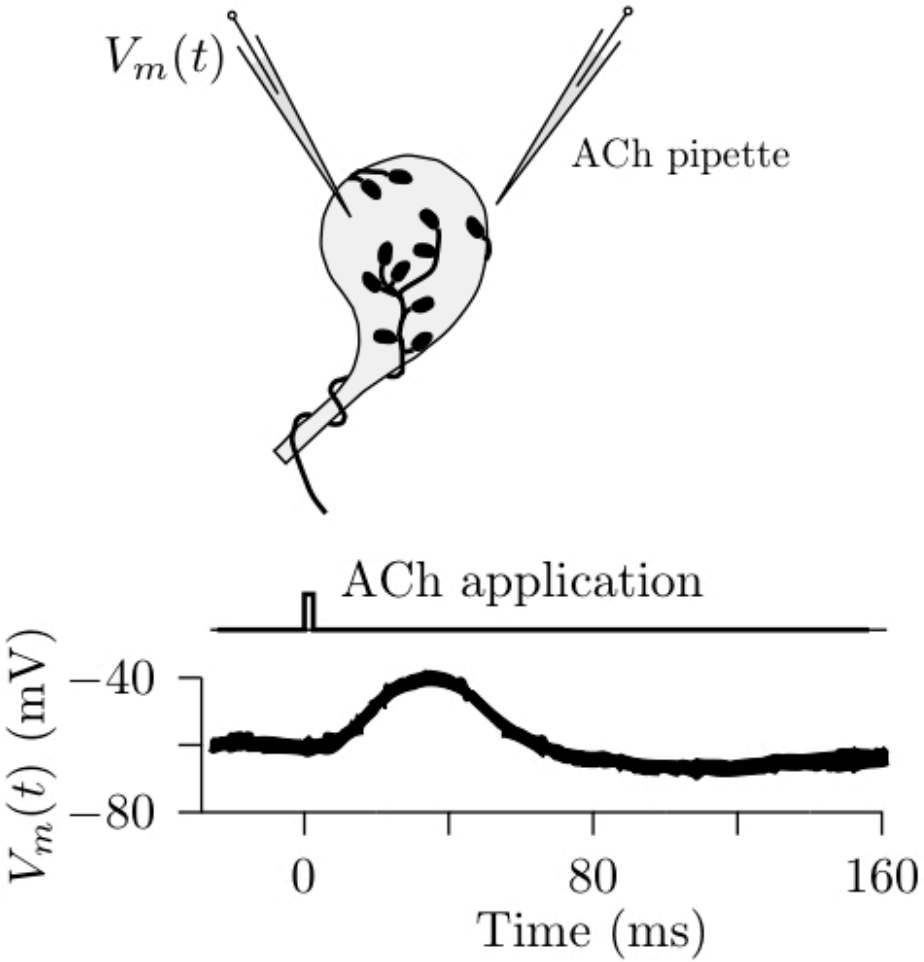

Figure 1.7

Action Potentials

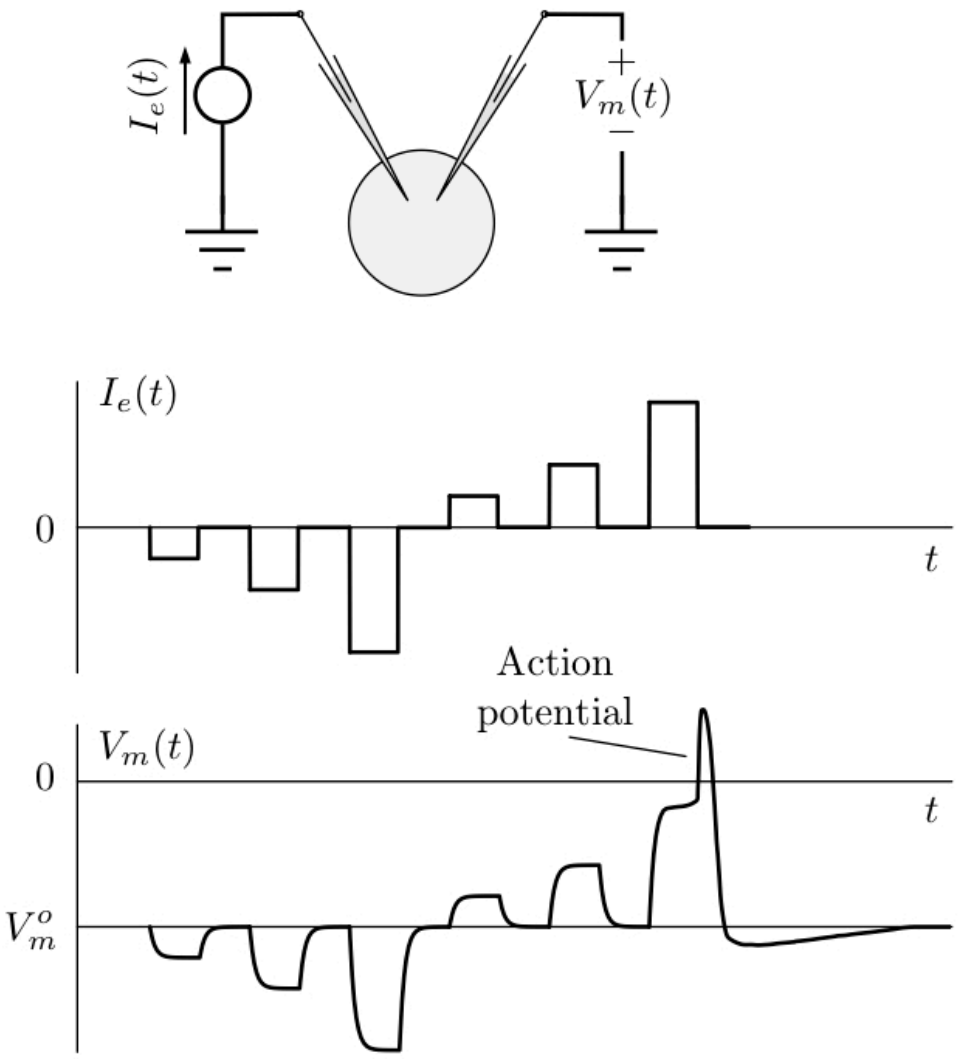

Figure 1.8

Not a graded potential!
(nonlinear; there is a *threshold*)

Graded vs Action Potentials

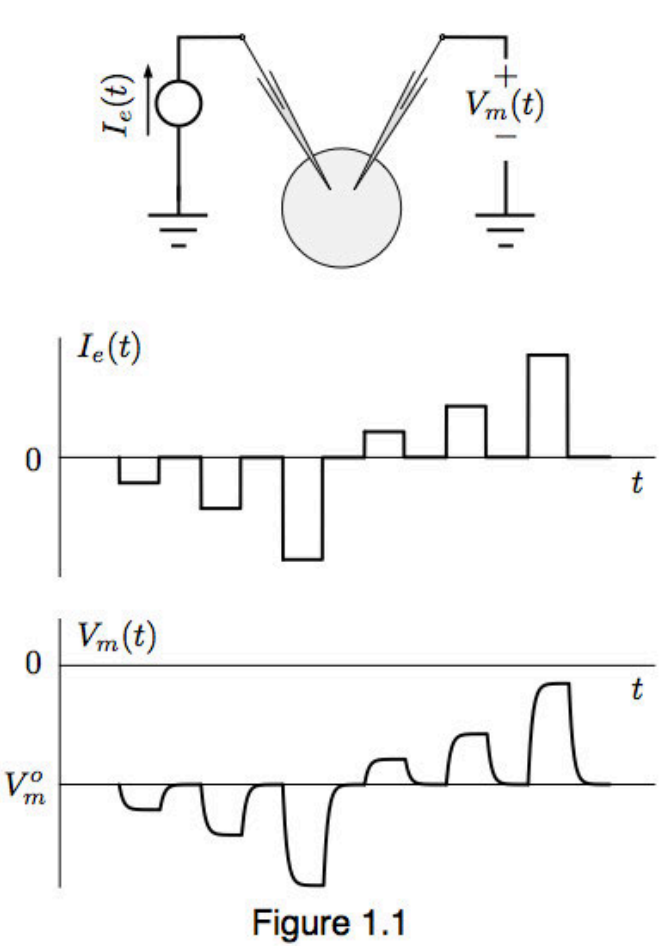

Figure 1.1

Electrically inexcitable cell

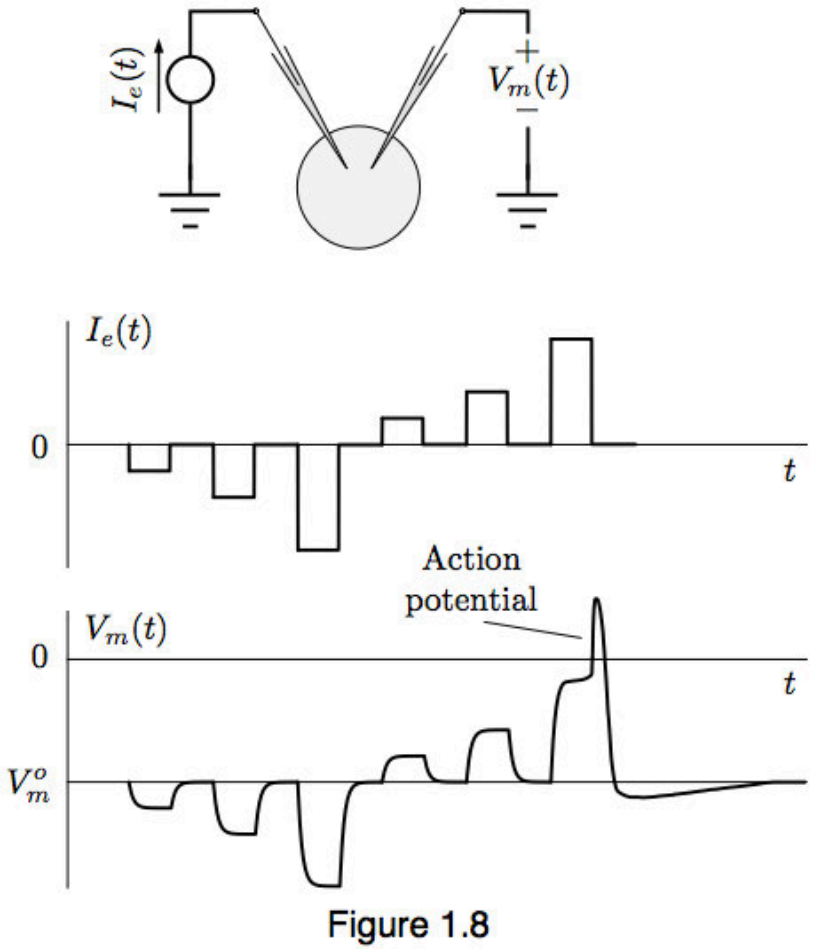

Figure 1.8

Electrically excitable cell

Action Potentials & Neurons

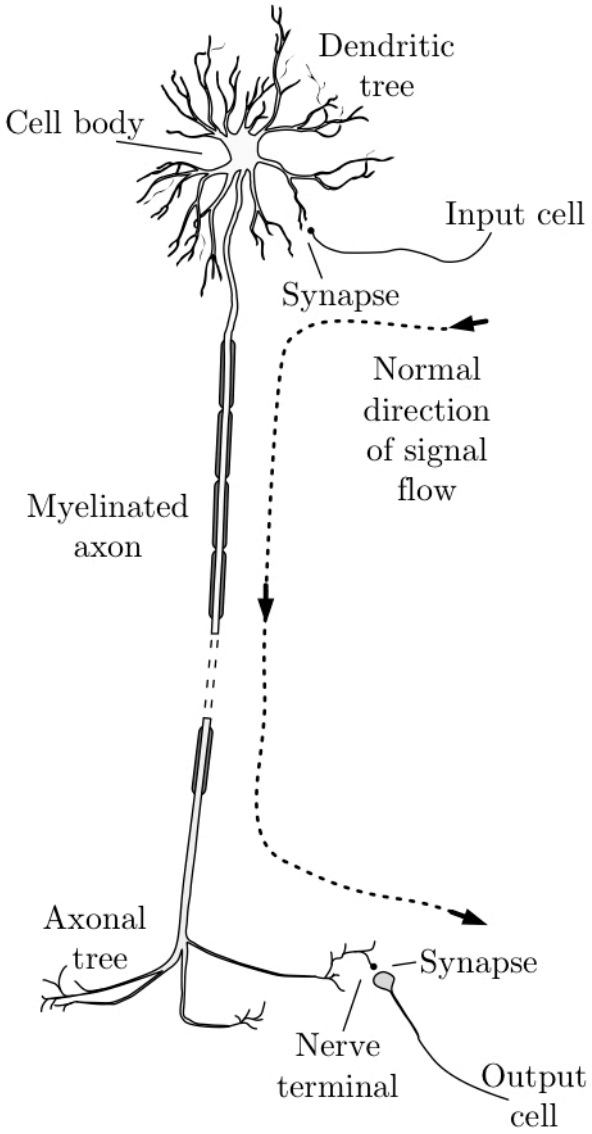

Figure 1.22

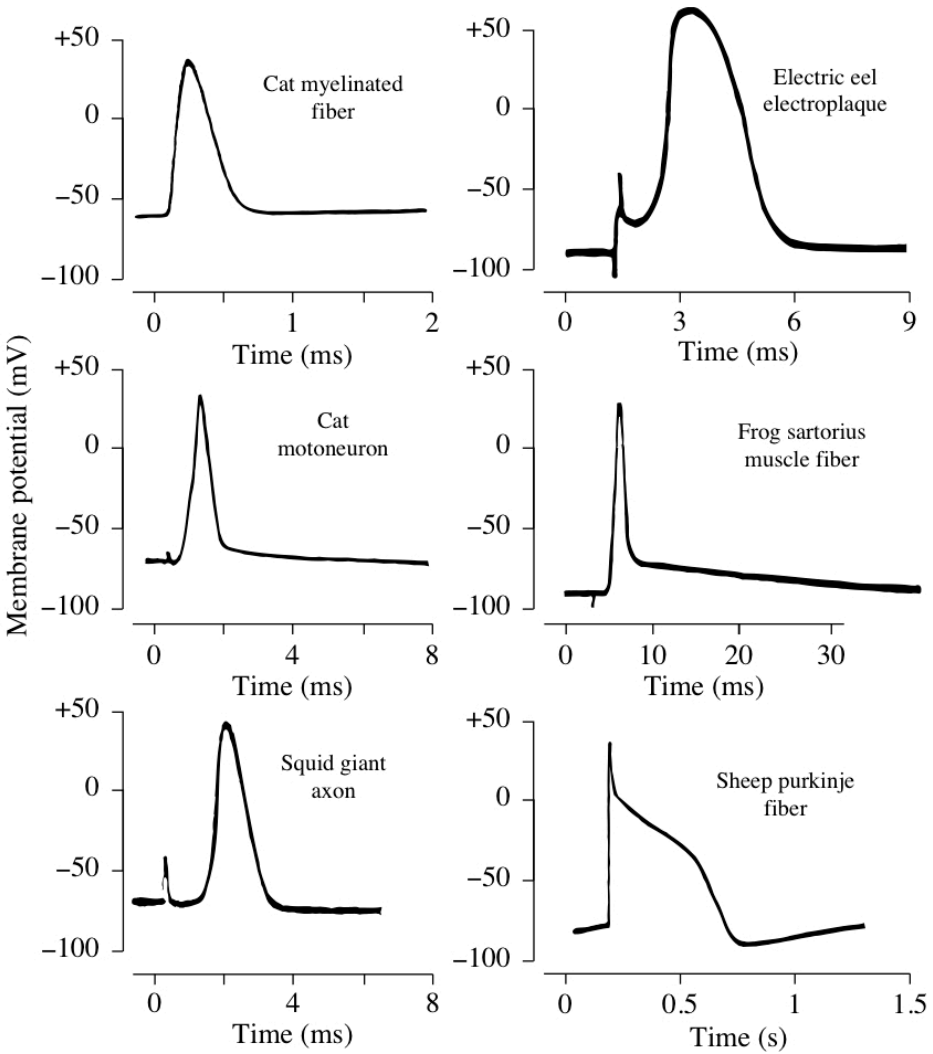

Figure 1.9

Action Potentials

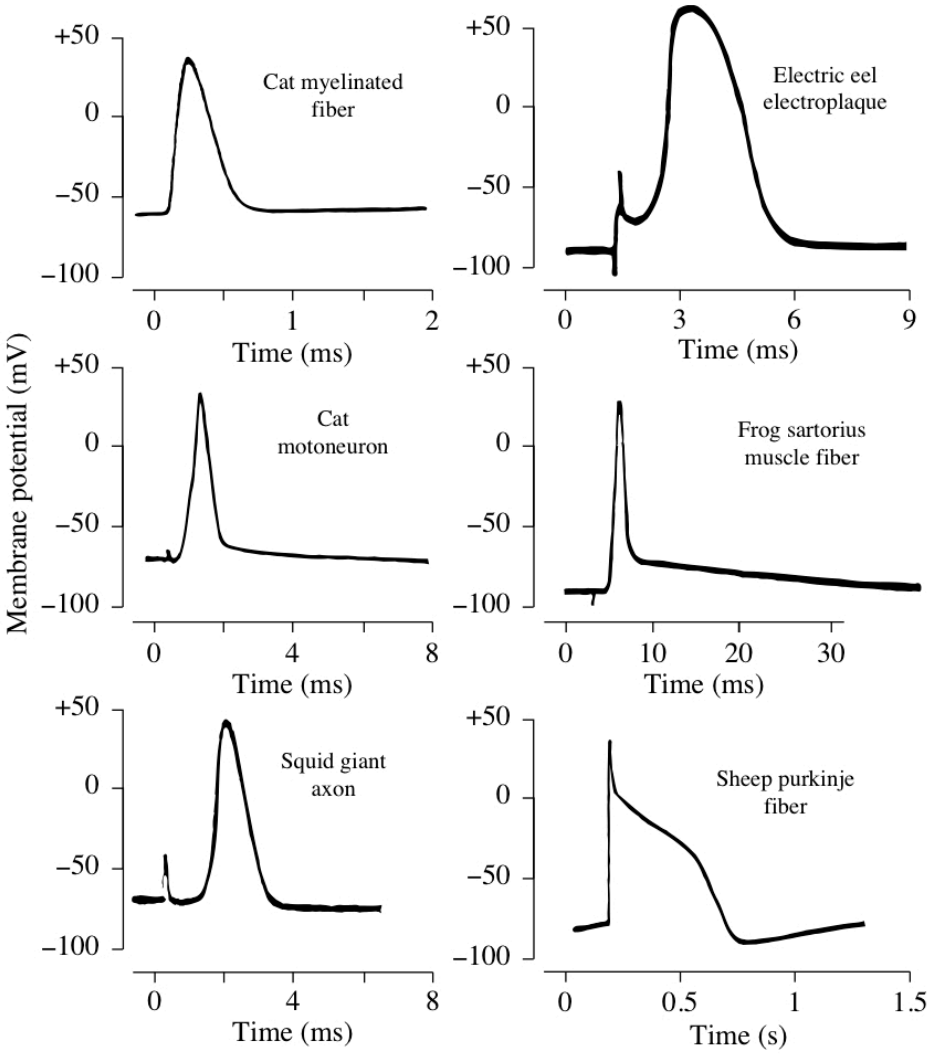

Figure 1.9

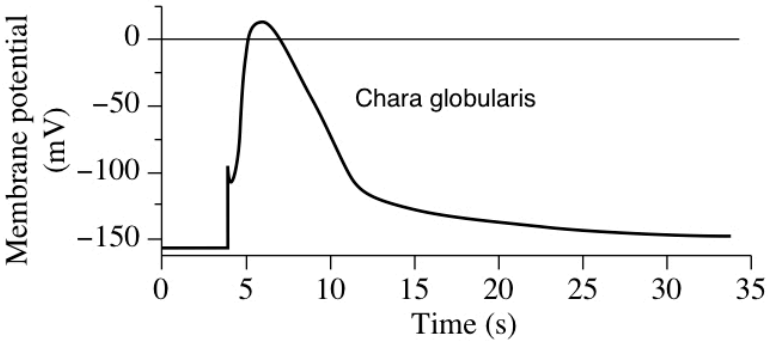

Figure 1.10

→ Wide range of timescales for an action potential 'firing'

“Neural code”

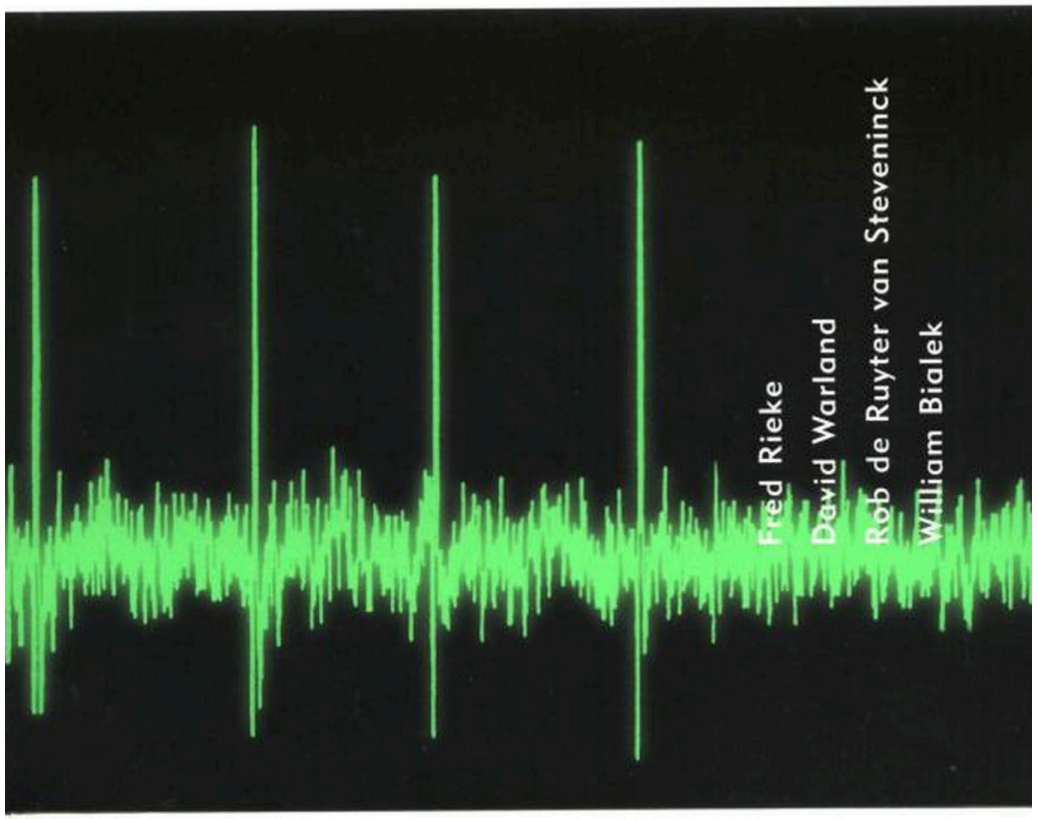
SPIKES
EXPLORING THE NEURAL CODE
Fred Rieke
David Warland
Rob de Ruyter van Steveninck
William Bialek

Ex. Neural coding of auditory stimuli

Guinea pig intracellular IHC responses

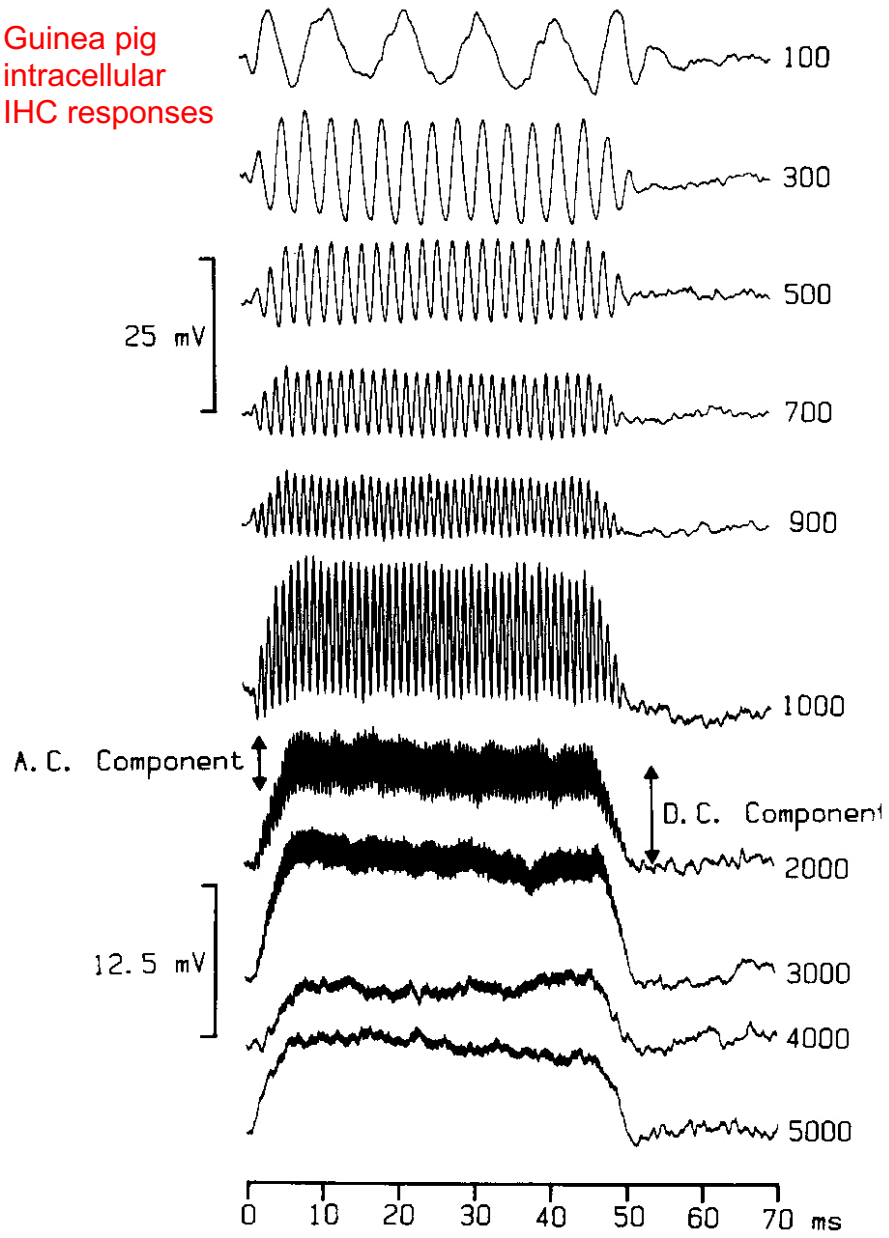

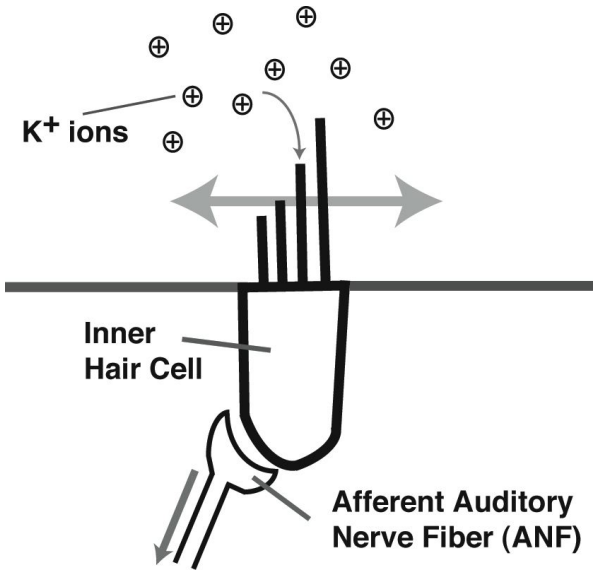

Transduction is nonlinear

- Hair cells act as low-pass filters (due to membrane capacitance)

→Hair cells (graded potentials) act as front end to auditory neurons (action potentials)

Palmer & Russell (1986)

Ex. Neural coding of auditory stimuli

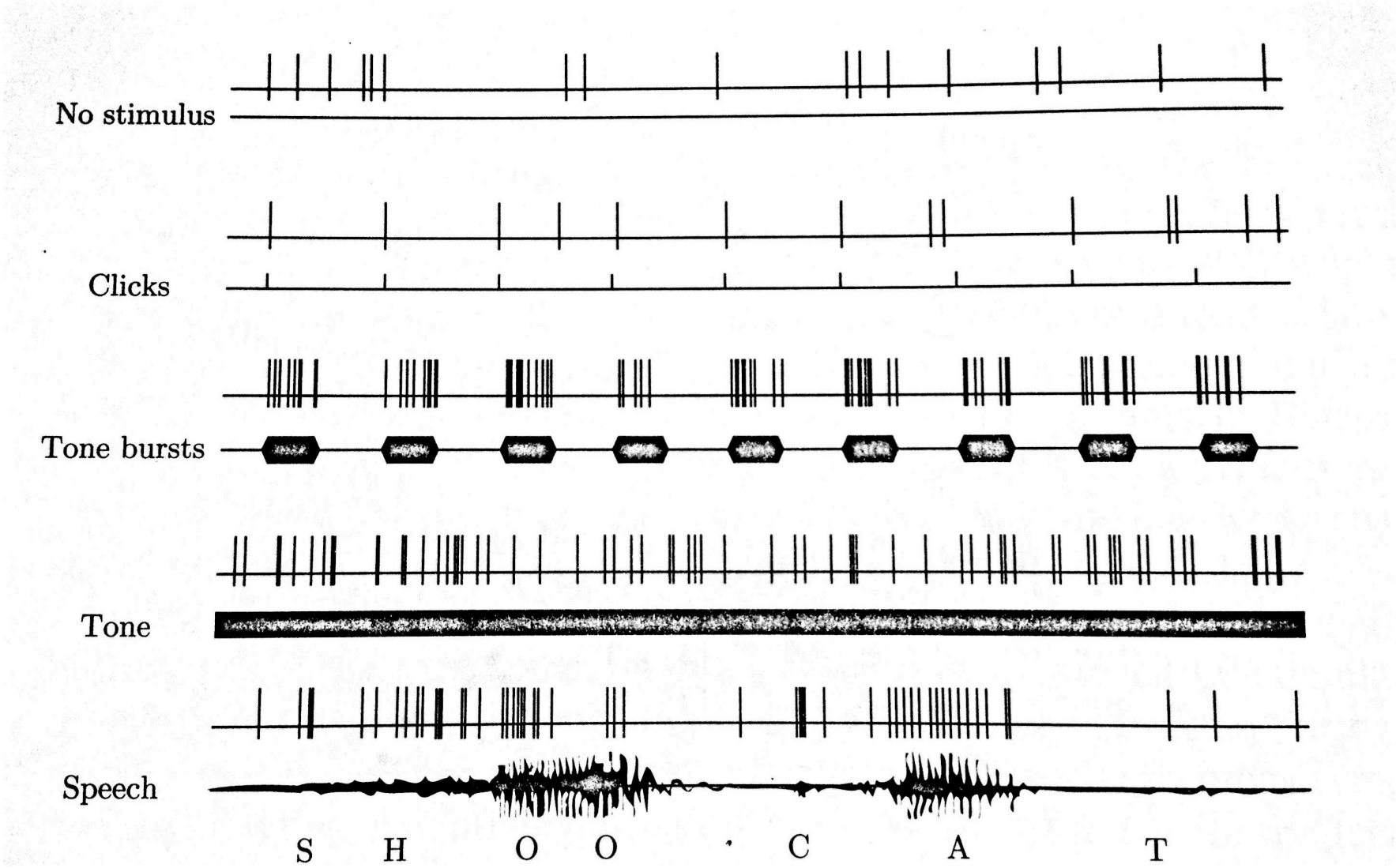

Kiang (1975)

“Neural code”

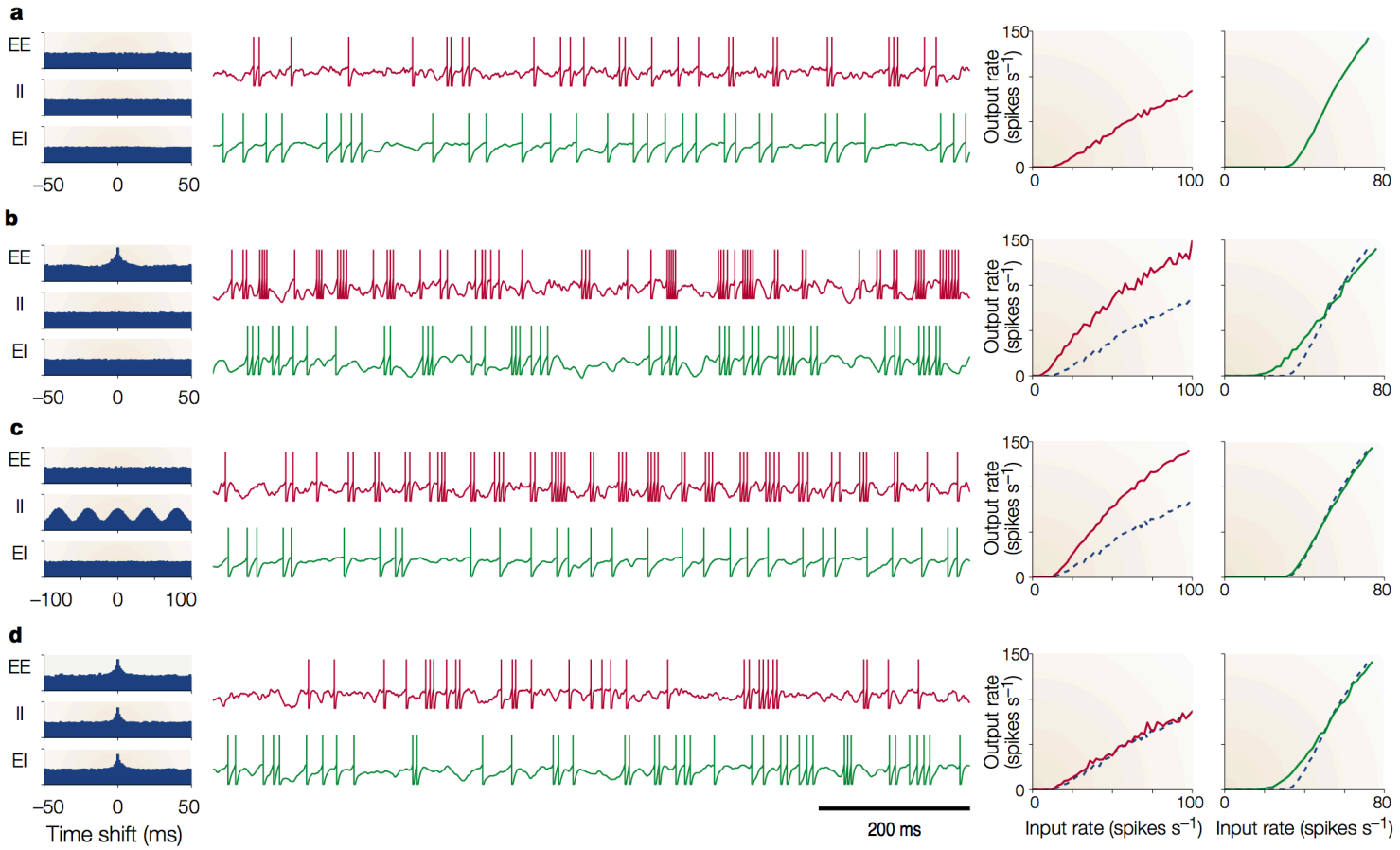

Figure 2 | **Responses of two model neurons to four input correlation patterns.** Histograms on the left show average cross-correlations, like those in FIG. 1, between pairs of excitatory inputs (EE), between pairs of inhibitory inputs (II), and between excitatory–inhibitory pairs (EI). The *y* axes in the correlograms extend from 0.7 to 1.4. Red and green traces correspond to responses of balanced and unbalanced neurons, respectively, always driven by 160 excitatory and 40 inhibitory inputs. The rate of inhibitory inputs was always 1.7 times the excitatory rate. In the middle traces, all excitatory inputs fired at 42 spikes s^{-1}. In the plots on the right, the mean firing rate of the excitatory inputs varies along the *x* axes, and the *y* axes correspond to the output firing rates of the two postsynaptic model neurons. All responses were obtained using leaky integrate-and-fire models (see BOX 1). **a** | All input spike trains were independent. In the middle traces, both postsynaptic neurons are shown to fire at about 30 spikes s^{-1}. **b** | Excitatory inputs were synchronous, with 10% shared inputs, as in FIG. 1a. Balanced and unbalanced neurons fired at 67 and 45 spikes s^{-1}, respectively. **c** | Inhibitory inputs oscillated with an amplitude equal to 50% of the mean rate, as in FIG. 1e. Balanced and unbalanced neurons fired at 59 and 30 spikes s^{-1}, respectively. **d** | All inputs were synchronous, with 10% shared inputs. Balanced and unbalanced neurons fired at 31 and 41 spikes s^{-1}, respectively. For comparison, broken lines in the input–output rate plots (**b**–**d**) are the curves obtained with independent inputs (**a**). The balanced neuron is much more sensitive to correlations than the unbalanced one.

Salinas & Sejnowski (2001)

“Neural code”

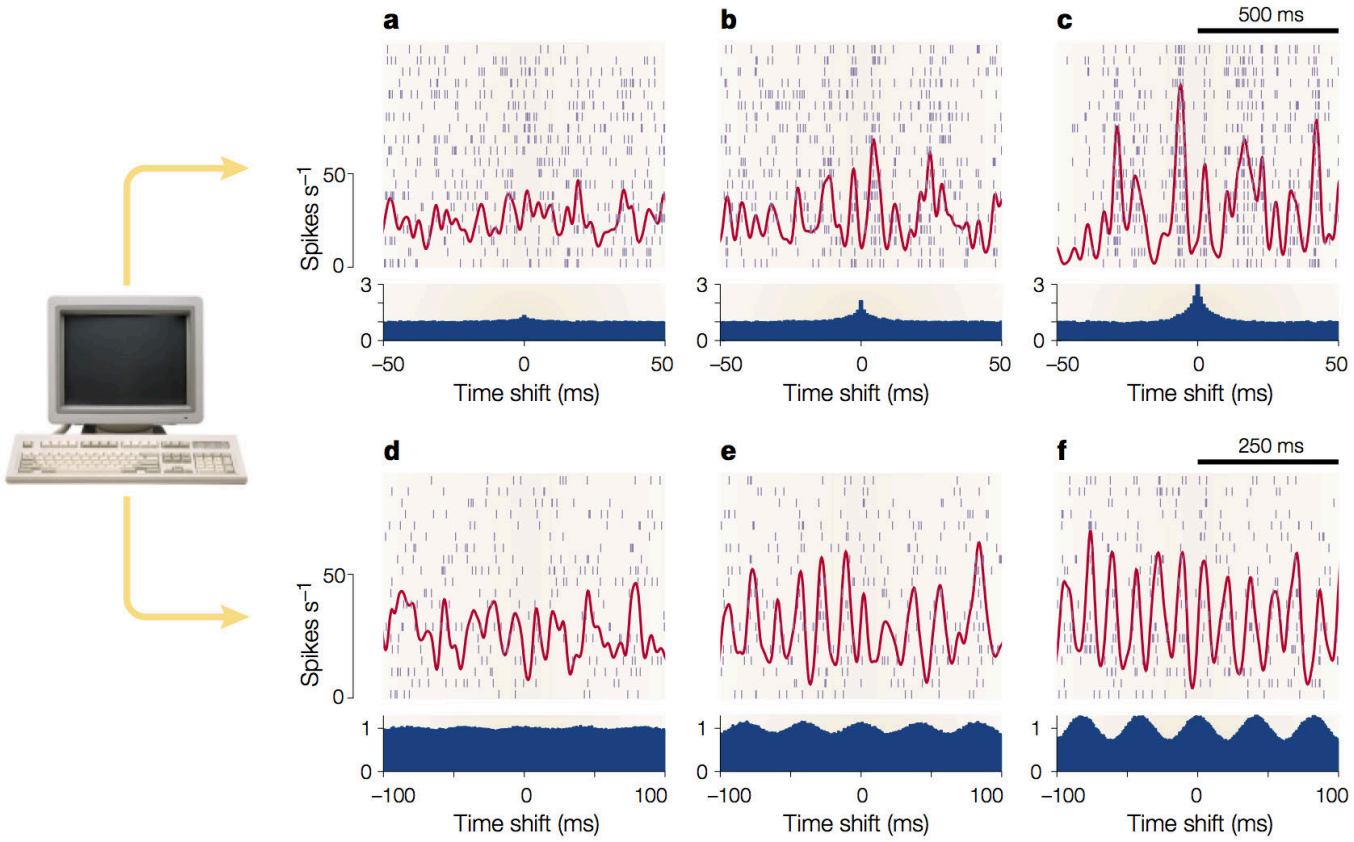

Figure 1 | **Synthetic computer-generated spike trains with various correlation patterns.** Each panel includes a raster plot with 20 simulated spike trains generated simultaneously; each row corresponds to one artificial neuron and each small vertical line to a spike. All neurons were set to fire at a mean rate of 27 spikes s^{-1} and with a CV_{ISI} near 1, as for a Poisson process (the CV_{ISI} is equal to the standard deviation of the interspike intervals divided by their mean). Red traces show instantaneous firing rate or spike density, obtained by smoothing the spike traces with a Gaussian function ($\sigma = 10$ ms for top row; $\sigma = 5$ ms for bottom row) and averaging across neurons. Blue histograms show the average cross-correlation between all possible distinct pairs of units. Cross-correlograms were computed from 20-s segments of simulated data, which included the short segments shown. The *y* axes are proportional to the probability that two spikes from two different neurons are separated in time by the amount indicated in the *x* axis. The normalization is such that the probability expected by chance, assuming independence, is set to 1. **a**–**c** | Each neuron was driven by 1,000 random inputs[52] and, on average, individual pairs of neurons shared 10% (**a**), 25% (**b**) or 50% (**c**) of those inputs. As the fraction of shared inputs rises, neurons tend to fire closer together in time, which produces larger fluctuations in the average spike density. **d**–**f** | Here, the neurons fired through independent Poisson processes, but the underlying firing rate was equal to $27(1 + A\sin(2\pi 25t))$, where *t* is the time in seconds, and was identical for all units. So, the mean rate was still 27 spikes s^{-1}, but it oscillated with a frequency of 25 Hz. The amplitude of the oscillations was $A = 0.25$ (**d**), $A = 0.50$ (**e**) or $A = 0.75$ (**f**). See REF. 52 for further details.

Salinas & Sejnowski (2001)

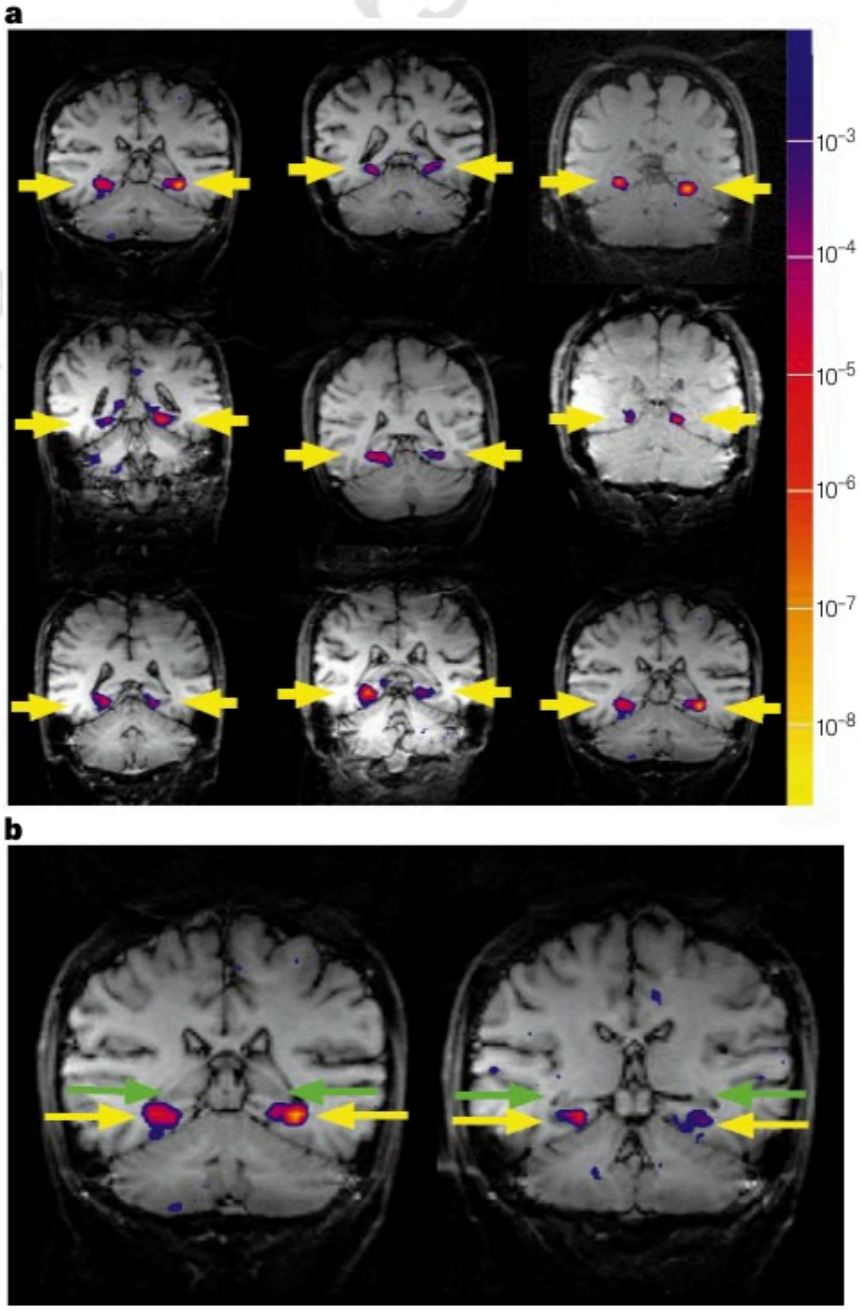

Epstein & Kanwisher (1998)

Ex. “Spike reliability”

“frozen noise”

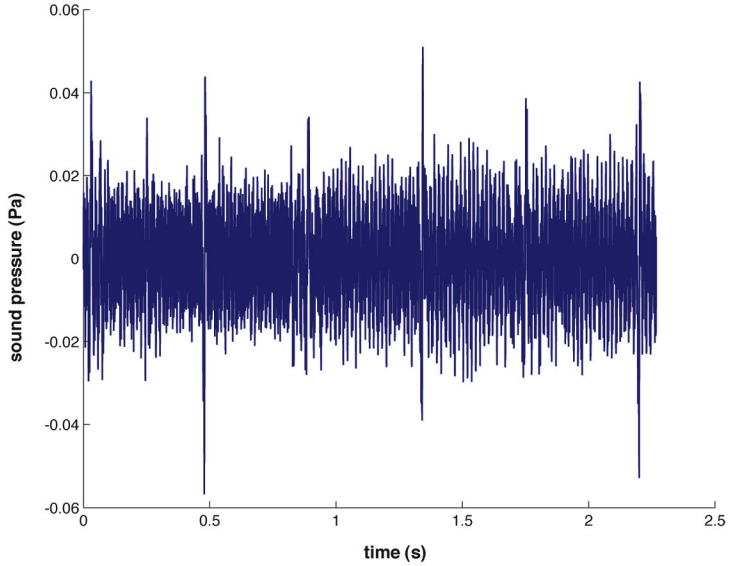

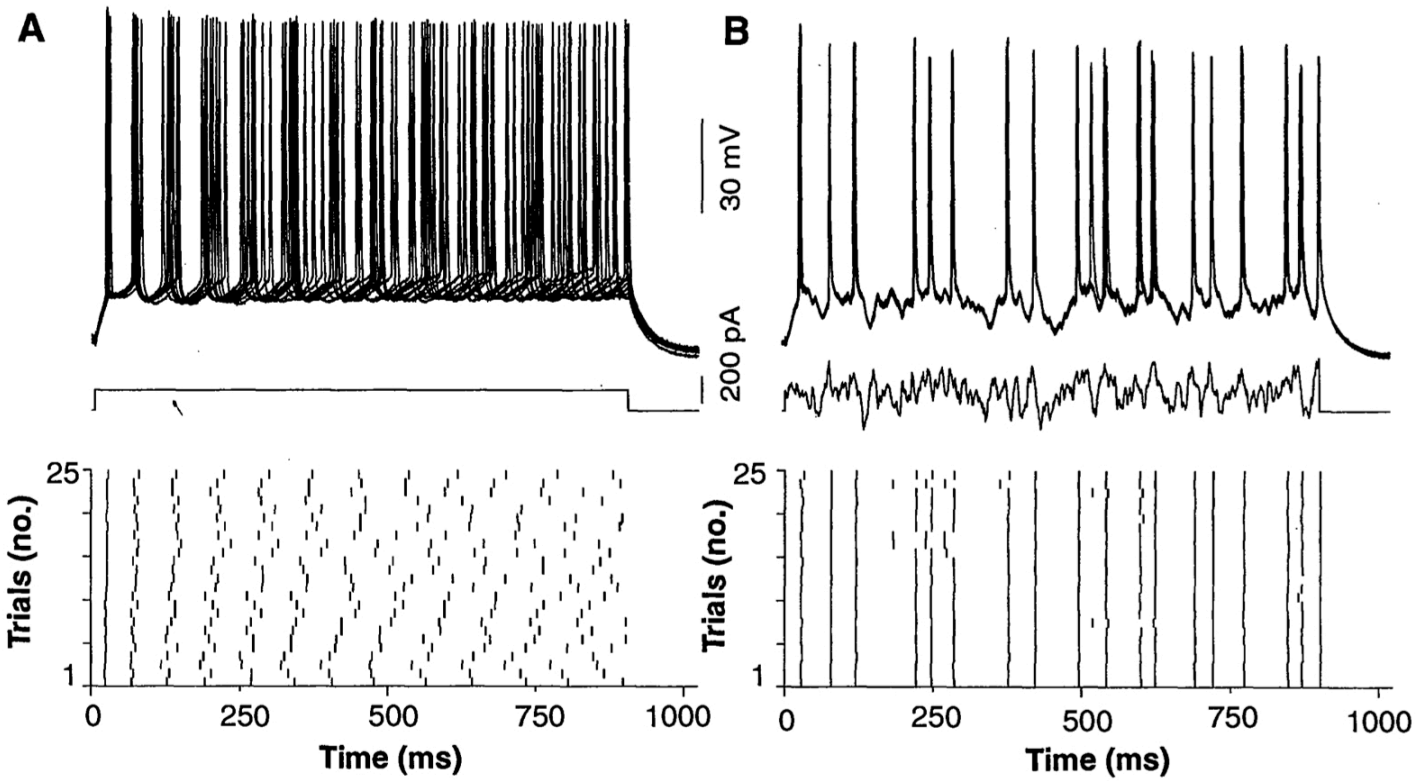

“spike reliability”

Mainen & Sejnowski (1995)

Ex. “Spike reliability”

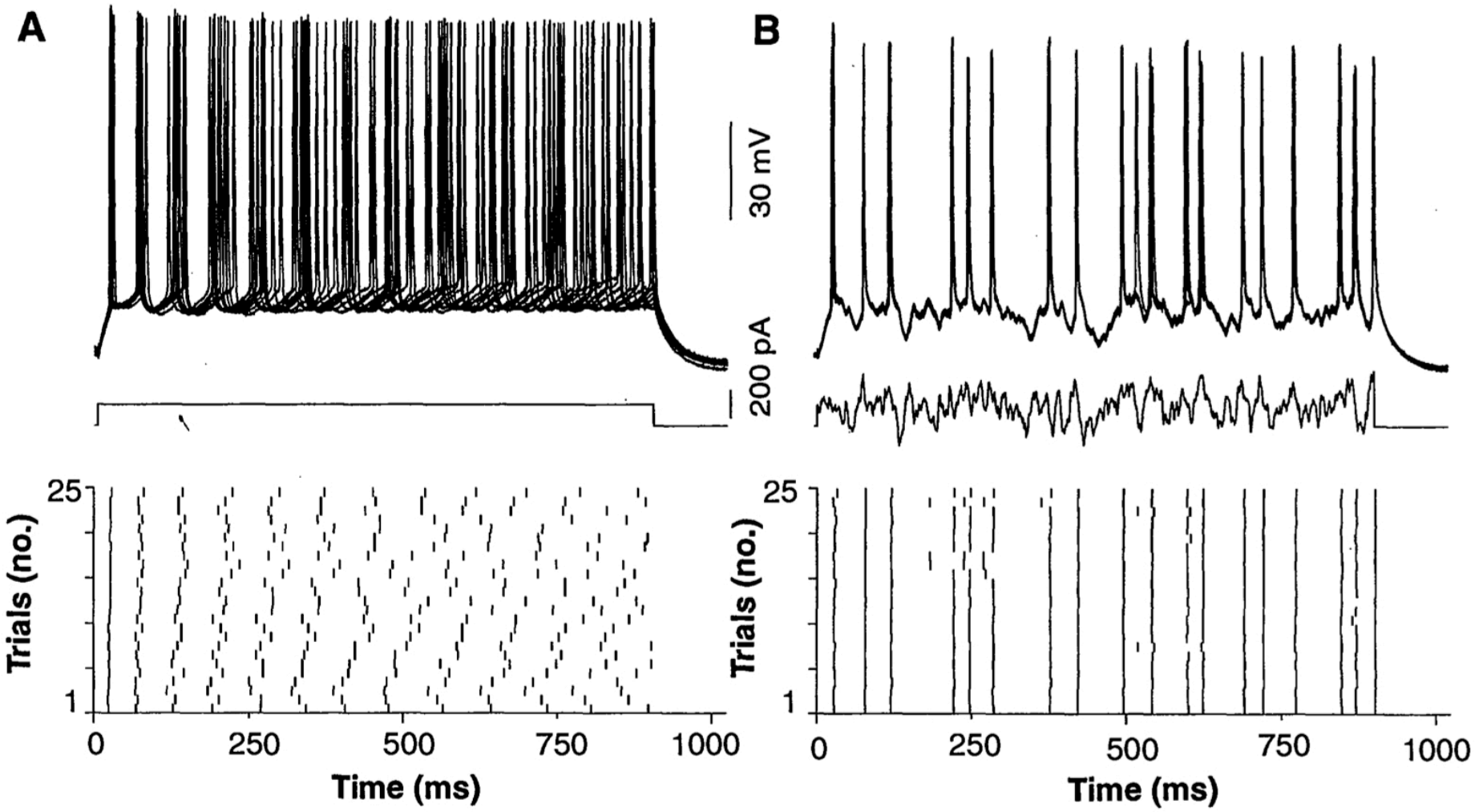

Mainen & Sejnowski (1995)

Looking Ahead: Hodgkin-Huxley network

Figure 4.7 (vol.2)

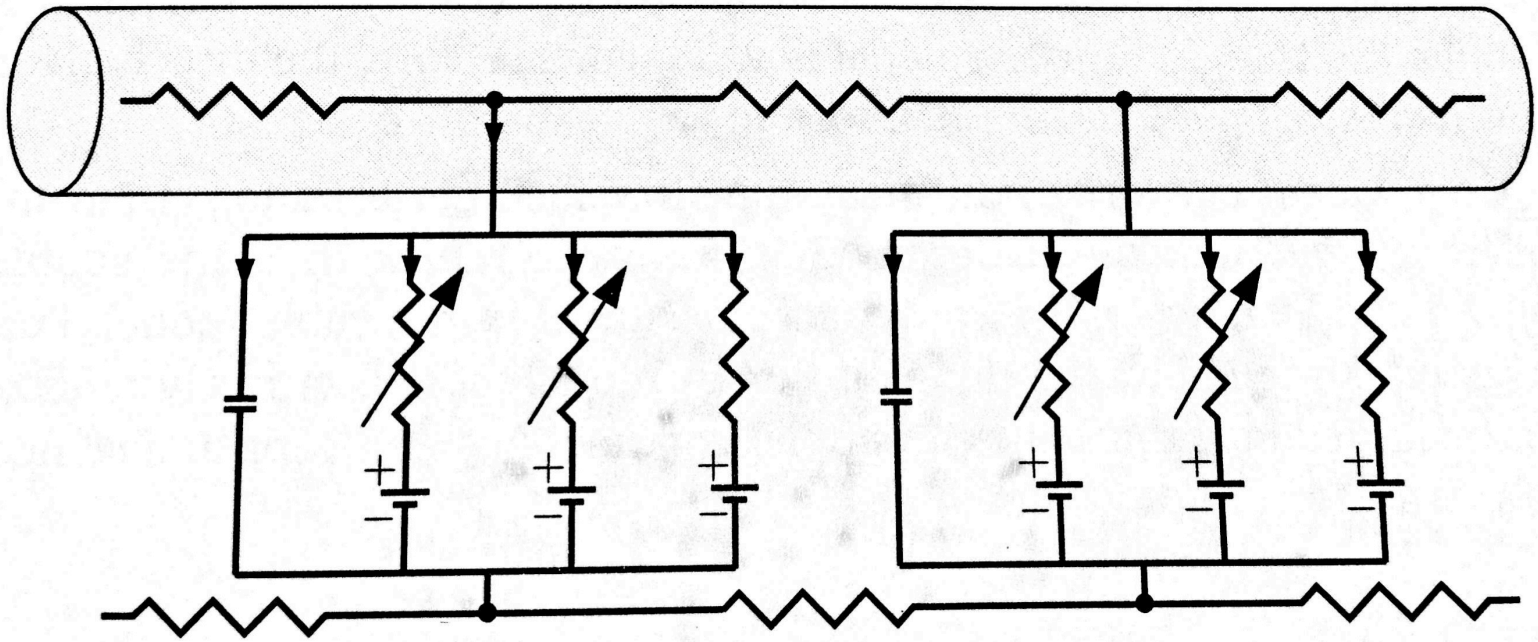

Two main ingredients:

- "sections" of membrane behaving like parallel circuit w/ variable conductances & a capacitor → action potentials

- successive elements spatially arranged like a "transmission line" → propagation

Spatial Conduction → Propagation

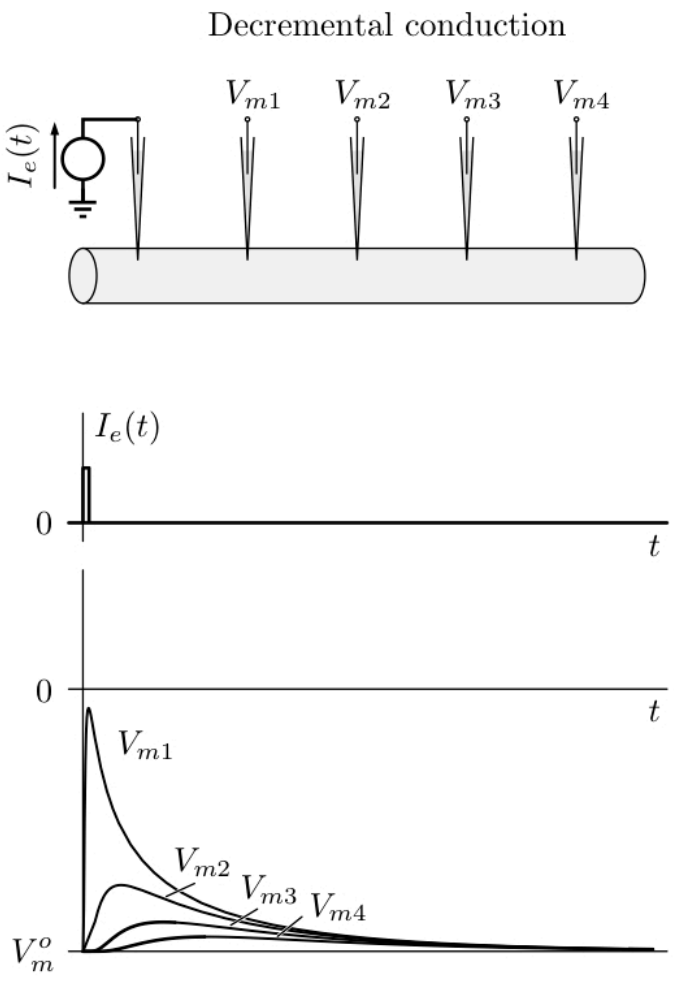

Electrically inexcitable cell

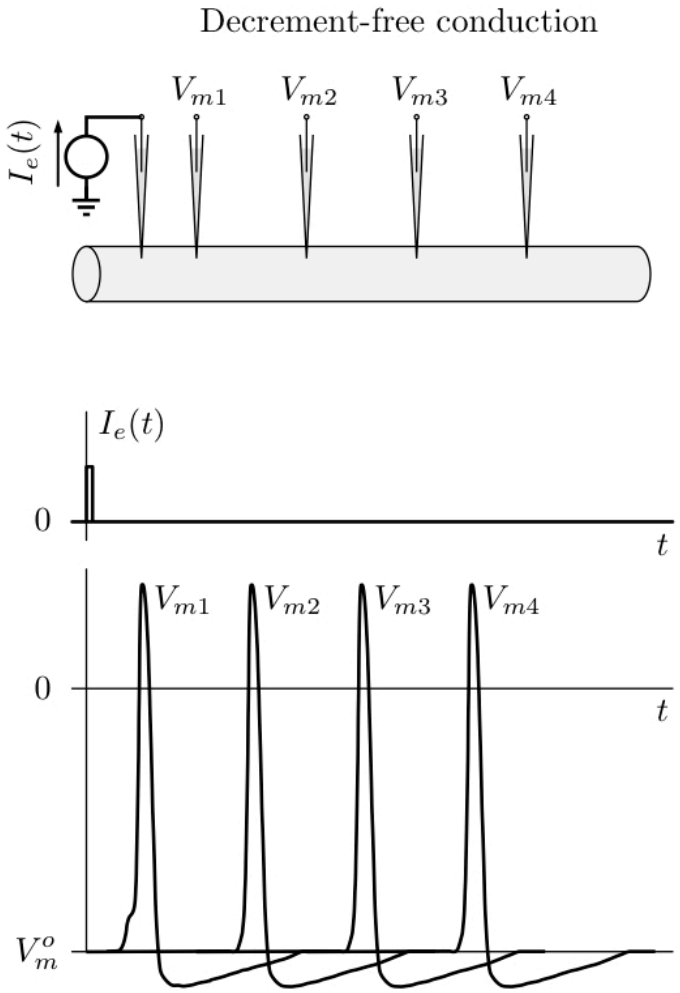

Electrically excitable cell